Coupled Thermal-Hydraulic-Mechanical Modelling of the Canister Retrieval Test

NWMO TR-2009-31 **October 2009**

R. Guo

Atomic Energy of Canada Limited

nwmo
NUCLEAR WASTE MANAGEMENT ORGANIZATION
SOCIÉTÉ DE GESTION DES DÉCHETS NUCLÉAIRES

Nuclear Waste Management Organization
22 St. Clair Avenue East, 6th Floor
Toronto, Ontario
M4T 2S3
Canada

Tel: 416-934-9814
Web: www.nwmo.ca

Coupled Thermal-Hydraulic-Mechanical Modelling of the Canister Retrieval Test

NWMO TR-2009-31

October 2009

R. Guo
Atomic Energy of Canada Limited

Disclaimer:

This report does not necessarily reflect the views or position of the Nuclear Waste Management Organization, its directors, officers, employees and agents (the “NWMO”) and unless otherwise specifically stated, is made available to the public by the NWMO for information only. The contents of this report reflect the views of the author(s) who are solely responsible for the text and its conclusions as well as the accuracy of any data used in its creation. The NWMO does not make any warranty, express or implied, or assume any legal liability or responsibility for the accuracy, completeness, or usefulness of any information disclosed, or represent that the use of any information would not infringe privately owned rights. Any reference to a specific commercial product, process or service by trade name, trademark, manufacturer, or otherwise, does not constitute or imply its endorsement, recommendation, or preference by NWMO.

ABSTRACT

Title: **Coupled Thermal-Hydraulic-Mechanical Modelling of the Canister Retrieval Test**
Report No.: **NWMO TR-2009-31**
Author(s): R. Guo
Company: Atomic Energy of Canada Limited
Date: October 2009

Abstract
One of the in-situ tests chosen for examination as part of a series of numerical simulations undertaken as part of the Engineered Barriers Systems Task Force (EBS-TF) is the Canister Retrieval Test (CRT) carried out in the Äspö Hard Rock Laboratory. The Canister Retrieval Test basically aims at demonstrating the readiness for recovering emplaced containers after the bentonite is fully saturated and has developed its maximum swelling pressure. The test also studied the thermal, hydraulic and mechanical evolution in the buffer from start until full water saturation. In the CRT, an electrically heated full-scale container was lowered into a deposition hole lined with blocks and rings of bentonite clay in the fall of 2000 and retrieved early in 2006, after five years of operation. A large number of instruments measured pressure, temperature and other parameters during this time. In order to evaluate the effectiveness of the CODE_BRIGHT modelling code in predicting the evolution of the coupled processes in unsaturated clay material, the one-dimensional and two-dimensional coupled thermal-hydraulic (TH) and coupled thermal-hydraulic-mechanical (THM) simulations for the CRT were conducted using CODE_BRIGHT. The simulated results are compared with measurements and presented in this report.

TABLE OF CONTENTS

Page

ABSTRACT ..... **v**

1. INTRODUCTION **1**

2. DESCRIPTION OF THE CANISTER RETRIEVAL TEST **1**

3. GEOMETRIES, BOUNDARY CONDITIONS AND INITIAL CONDITIONS **7**

3.1 ONE-DIMENSIONAL MODEL **7**
3.1.1 Geometry for One-Dimensional Model 7
3.1.2 Boundary Conditions and Initial Conditions for One-Dimensional Model 7
3.1.2.1 Boundary Conditions 7
3.1.2.2 Initial Conditions 9
3.2 TWO-DIMENSIONAL MODEL **9**
3.2.1 Geometry for Two-Dimensional Model 9
3.2.2 Boundary Conditions and Initial Conditions for Two-Dimensional Model 9
3.2.2.1 Boundary Conditions 9
3.2.2.2 Initial Conditions 10
3.3 MATERIAL PARAMETERS **12**
3.3.1 Hydraulic Parameters of Materials 12
3.3.2 Thermal Parameters of Materials 13
3.3.3 Mechanical Parameters of Materials 13

4. MODELLING RESULTS AND COMPARISON WITH MEASUREMENTS **15**

4.1 MODELLING RESULTS FROM ONE-DIMENSIONAL MODEL AND COMPARISON WITH MEASUREMENTS **15**
4.1.1 Temperatures 15
4.1.1.1 Simulated Temperatures 15
4.1.1.2 Comparison of Temperatures between Simulations and Measurements 17
4.1.2 Hydraulic Response 19
4.1.2.1 Simulated Hydraulic Response in the Bentonite Materials 19
4.1.2.2 Comparisons of Simulated Hydraulic Response with Measurements 21
4.1.3 Mechanical Response 23
4.1.4 Summary of the Results from One-Dimensional Modelling 23
4.2 MODELLING RESULTS FROM TWO-DIMENSIONAL MODEL AND COMPARISON WITH MEASUREMENTS **24**
4.2.1 Thermal Response 24
4.2.1.1 Simulated Thermal Response in the Bentonite Materials 24
4.2.1.2 Comparison of Temperatures between Simulated Results and Measurements in the Bentonite Materials 28
4.2.1.3 Comparison of Temperatures between the Simulated Results and Measurements in the Rock 30
4.2.2 Hydraulic Response 33
4.2.2.1 Simulated Hydraulic Response in the Bentonite Materials 33
4.2.2.2 Comparison of Hydraulic Response between Simulated Results and Measurements 35
4.2.3 Mechanical Response 39
4.2.4 Summary of the Results from Two-Dimensional Modelling 40

4.3 COMPARISON OF MODELLING RESULTS FROM THE 1-D MODEL AND THE 2-D MODEL....41

5. CONCLUSIONS....42

ACKNOWLEDGEMENTS....42

REFERENCES....43

LIST OF TABLES

Page

Table 1: Mechanical Parameters used for Bentonite Materials in Coupled THM Modelling 14
Table 2: Mechanical Parameters used for Concrete Plug, Steel Lid and Bentonite Pellets.....15

LIST OF FIGURES

Page

Figure 1: Illustration of the Experimental Set-up of the Canister Retrieval Test and the Location in the TASD Tunnel 2
Figure 2: Schematic View Showing the Experiment Layout. Sensors have been placed in five of the bentonite blocks. For each block the number of each sensor type is described. (T=temperature, P=total pressure cell, U=pore pressure cell and W=relative humidity sensor).....3
Figure 3: Schematic Drawing of the Container Hole with Bentonite Blocks with Dimensions in mm.....4
Figure 4: Container Power Protocol of the CRT 5
Figure 5: Filter Mat Pressure Protocol of the CRT 5
Figure 6: Locations of Measurement Instruments in the Bentonite Rings, Bentonite Bricks, and Bentonite Cylinders.....6
Figure 7: Geometry for One-Dimensional Model.....7
Figure 8: Mesh for One-Dimensional Model.....8
Figure 9: Measured Temperatures at Locations of Sensors P12 and TR125 8
Figure 10: Dimensions of the Two-Dimensional Model 10
Figure 11: Meshes of the Two-Dimensional Model 11
Figure 12: Simulated Temperatures at Locations with Radial Distances of 540 mm, 635 mm, 735 mm, 815 mm and 847.5 mm from the Container Axis 15
Figure 13: Simulated Temperature at Locations with Radial Distances of 585 mm, 685 mm, 785 mm and 825 mm from the Container Axis 16
Figure 14: Profiles of Simulated Temperatures at Times of Day 670, Day 1400, Day 1800 and Day 1910 16
Figure 15: Simulated Temperature Contours in the Empty Gap, Bentonite Ring and Bentonite Pellets at Four Different Times.....17
Figure 16: Comparison of Temperatures between Simulated Results and Measurements at Sensors of T111, T121 and T112 18
Figure 17: Comparison of Temperatures between Simulated Results and Measurements during the First 600 days and Predicted Temperatures after 600 Days at Sensors of W119, W120 and W121 18
Figure 18: Simulated Water Saturations at Locations with Radial Distances of 540 mm, 635 mm, 735 mm, 815 mm and 847.5 mm from the Container Axis.....19
Figure 19: Simulated Water Saturation Histories at Locations with Radial Distances of 585 mm, 685 mm, 785 mm and 825 mm from the Container Axis.....19
Figure 20: Simulated Degree of Saturation in the Unfilled Annular Gap.....20
Figure 21: Simulated Pore Water Pressures in the Empty Gap, Bentonite Ring and Bentonite Pellets at Four Different Times.....21

continued…

LIST OF FIGURES

Page

Figure 22: Comparison of Simulated Relative Humidiity with Measurements during the First 600 Days and Predicted Relative Humidities after 600 Days at Locations of W119, W120 and W121 22
Figure 23: Comparison of Simulated Suctions with Measurements at Locations of W122, W123 and W124 22
Figure 24: Simulated Vertical Stresses vs. Time at Different Locations 23
Figure 25: Comparison of Simulated Vertical Stresses and Measurements at Locations of P110, P111 and U106 24
Figure 26: Simulated Temperatures at Different Radial Distances along Level C3 25
Figure 27: Profiles of Simulated Temperatures at Four Different Times along Level C3 25
Figure 28: Simulated Temperatures at Different Radial Distances along Level R10 26
Figure 29: Simulated Temperature Profiles along Level R10 at Four Different Times 26
Figure 30: Simulated Temperature Histories at Different Radial Distances along Level R5 27
Figure 31: Profiles of Simulated Temperatures along Level R5 at Four Different Times 27
Figure 32: Simulated Temperature Contours in the Bentonite Ring, Bentonite Bricks, Bentonite Pellets and Cylindrical Bentonite at Four Different Times 28
Figure 33: Comparison of Temperatures between Simulated Results from 2-D Model and Measurements at Sensors of T111, T121 and T112 29
Figure 34: Comparison of Measured Temperatures and Predicted Temperatures during the First 600 Days at Sensors of W119, W120 and W121 29
Figure 35: Comparison of the Simulated and Measured Temperatures at Two Different Locations T127 (in R10) and T129 (in C3) 30
Figure 36: Locations at which Temperatures in the Rock were Measured 31
Figure 37: Comparison of Simulated Temperatures with Measurements at Locations of TR105 and TR108 in the Rock 31
Figure 38: Comparison of Simulated Temperatures with Measurements at Locations of TR117 and TR120 in the Rock 32
Figure 39: Comparison of Simulated Temperatures with Measurements at Locations of TR129 and TR132 in the Rock 32
Figure 40: Simulated Water Saturation Histories at Different Locations along Level R10 33
Figure 41: Simulated Water Saturation Profiles along Level R10 33
Figure 42: Simulated Water Saturation Histories at Different Locations along Level C3 34
Figure 43: Simulated Water Saturation Profiles along Level C3 34
Figure 44: Simulated Pore Water Pressure Contours in the Bentonite Ring, Bentonite Bricks and Cylindrical Bentonite at Four Different Times 35
Figure 45: Comparisons of Simulated Relative Humidity with Measurements at Locations W134, W142, W137, W151 and W153 36
Figure 46: Comparison of Simulated Water Saturation with Measured Results along Level R6 36
Figure 47: Comparison of Simulated Water Saturation with Measured Results along Level R7 37
Figure 48: Comparison of Simulated Water Saturation with Measured Results along Level R10 37
Figure 49: Comparison of Simulated Water Saturation with Measured Results along Level C3 38

continued…

LIST OF FIGURES (Concluded)

Page

Figure 50: Comparison of the Simulated Relative Humidity with Measurements during the First 600 Days and Predicted Relative Humidities after 600 Days at Location of W119, W120 and W121 38
Figure 51: Comparison of the Simulated Suction with Measurements at Location of W122, W123 and W124 39
Figure 52: Comparison of the Simulated Vertical Stresses and Measured Results at Locations of P110, P111 and U106 40
Figure 53: Comparison of the Simulated Vertical Stresses and Measured Results at Locations of P119 and P125 41
Figure 54: Comparison of Temperatures from 1-D Model and from 2-D Model 42

1. INTRODUCTION

One option for the long-term management of used nuclear fuel involves placement of used-fuel containers (referred to as canisters in the SKB and Posiva concepts), in a repository located in a deep geologic medium. In this concept, containers will be separated from the surrounding rock by a placement-room sealing system (e.g., composed primarily of clay-based buffer with or without aggregates). One function of the sealing system is to minimize the rate of groundwater movement within the sealed placement room. In many repository concepts bentonite clay is proposed for use as one of the sealing materials because when adequately compacted it: possesses very low hydraulic conductivity and the ability to swell in the presence of water, thereby closing potential flow path. It also has useful chemical (i.e., high cation exchange capacity (CEC)) and physical attributes. Considerable effort is being expended in performing both laboratory and in-situ tests at different scales and in developing, verifying and validating mathematical models of the coupled processes that can be used to describe/simulate the observed laboratory and field behaviour (Alonso et al. 1990; Chandler 2003; ENRESA 2000; Gens et al. 1998; Graham et al. 1997; Thomas et al. 2003; Villar 2002; Gray et al. 1985; Kristensson and Borgesson 2008).

One of the in-situ tests associated with development of the deep geological disposal concept in Sweden is the Canister Retrieval Test (CRT), carried out in the Äspö Hard Rock Laboratory (Kristensson and Borgesson 2008). The Canister Retrieval Test is intended to demonstrate the retrievability of emplaced containers after the bentonite is fully saturated and has developed its maximum swelling pressure. However, the test is also useful in studying the thermal, hydraulic and mechanical evolution in the buffer (i.e., bentonite materials installed immediately adjacent to the container) from start until full water saturation. In the CRT, an electrically heated full-scale container was lowered into a deposition hole lined with blocks and rings of bentonite clay in the fall of 2000 and retrieved after five years exposure early in 2006. The bentonite next to the container had been saturated with groundwater at the end of the test. A large number of instruments measured pressure, temperature and other parameters during this time. In order to evaluate the effectiveness of several mathematical models in predicting the evolution of the coupled processes in unsaturated clay material, the results from the CRT are shared among international numerical groups (Engineering Barrier System Task Force modeling group (EBS TF modeling group)) for these groups to compare their modeling results to the results of the heated test. Atomic Energy of Canada Limited (AECL), representing the Nuclear Waste Management Organization, is a member of the EBS TF modeling group.

2. DESCRIPTION OF THE CANISTER RETRIEVAL TEST

A schematic view of the CRT is given in Figure 1. Figures 2 and 3 show schematic layouts of the experiment and its dimensions. The CRT is installed in a vertical borehole drilled in the bottom of a horizontal tunnel in granite in the Äspö Hard Rock Laboratory. It is 6 m between the centre of the CRT and the centre of the Temperature Buffer Test (TBT). The tunnel cross section has the approximate dimensions of 6-m x 6-m with a horseshoe shape. There are 16 filter mats of 10-cm-width installed uniformly around the perimeter of the borehole from 0.15 m from the bottom to 6.25 m height. Under the bottom of the container, there is a 0.5-m-thick cylindrical bentonite block (C1). Vertically 0.5-m-thick ring-shaped blocks with a radial thickness of 0.285 m (R1 through R10) are placed in the space between the container and the granite. There is a 10-mm-thick gap between the outer surface of the container and the inside

surface of the ring-shaped blocks. The volume between the top surface of the container and the top surface of the upper most ring (R10) is filled with about 220~230-mm-thick bentonite bricks as shown in Figure 3. Three layers of 0.5-m-thick cylindrical bentonite blocks (C2, C3 and C4) are placed between the top surface of the bentonite bricks and the bottom of the retaining concrete plug. Bentonite pellets fill the gap between the bentonite blocks and the filter mats. An impermeable rubber seal is installed between bentonite blocks C4 and the bottom of the concrete plug. A steel lid is installed on the top of the plug. The plug and the lid are restrained vertically by nine rock anchors.

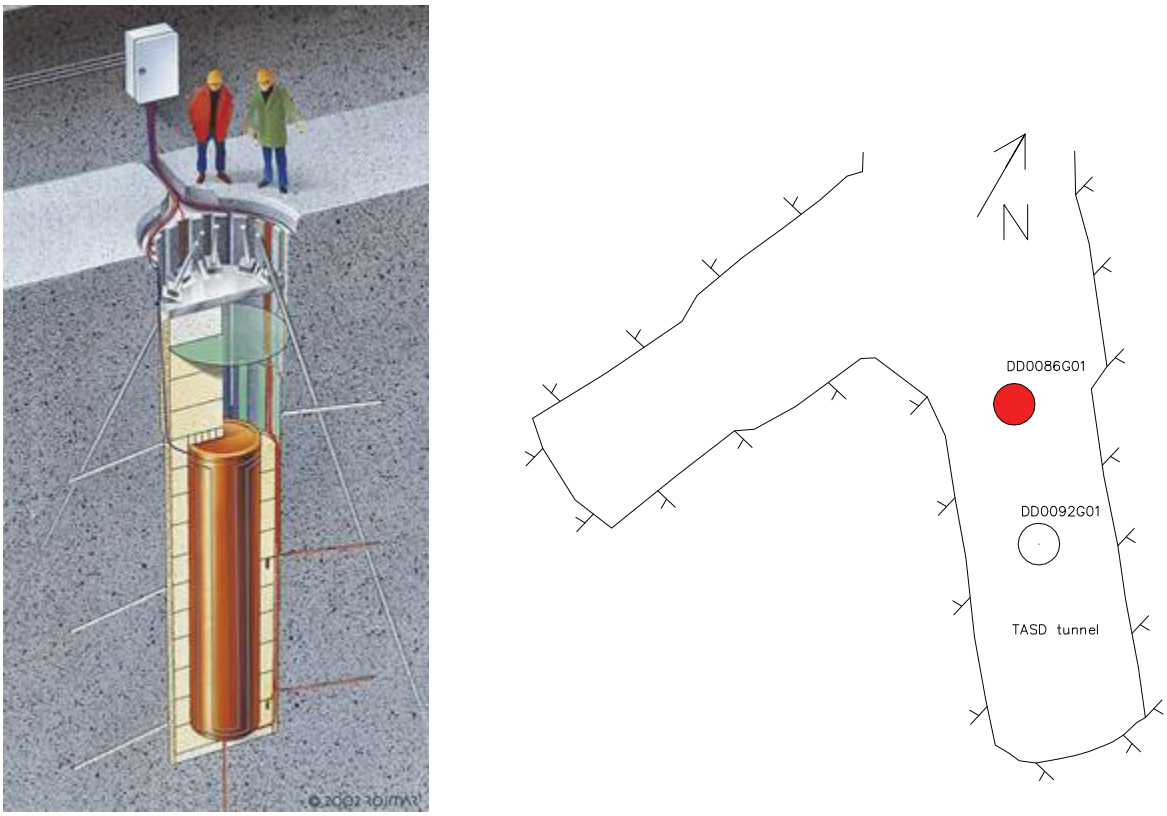

Figure 1: Illustration of the Experimental Set-up of the Canister Retrieval Test and the Location in the TASD Tunnel[1]

The test was installed in autumn 2000. Heating was started with an initially constant power of 700 W on October 23, 2000 (day 1), one day after casting the concrete plug. The container heating power was raised twice: to 1700 W on November 13 and to 2600 W on February 13. The detailed heater power protocol can be found in Figure 4. The power of the heaters in the container was reduced to 2100 W on day 683 and to 1600 W on day 1135 (December 4, 2003). The later reduction was done on day 1596 to 1150 W.

[1] O. Kristensson, L. Börgesson. CRT-canister retrieval test: EBS task force assignment.

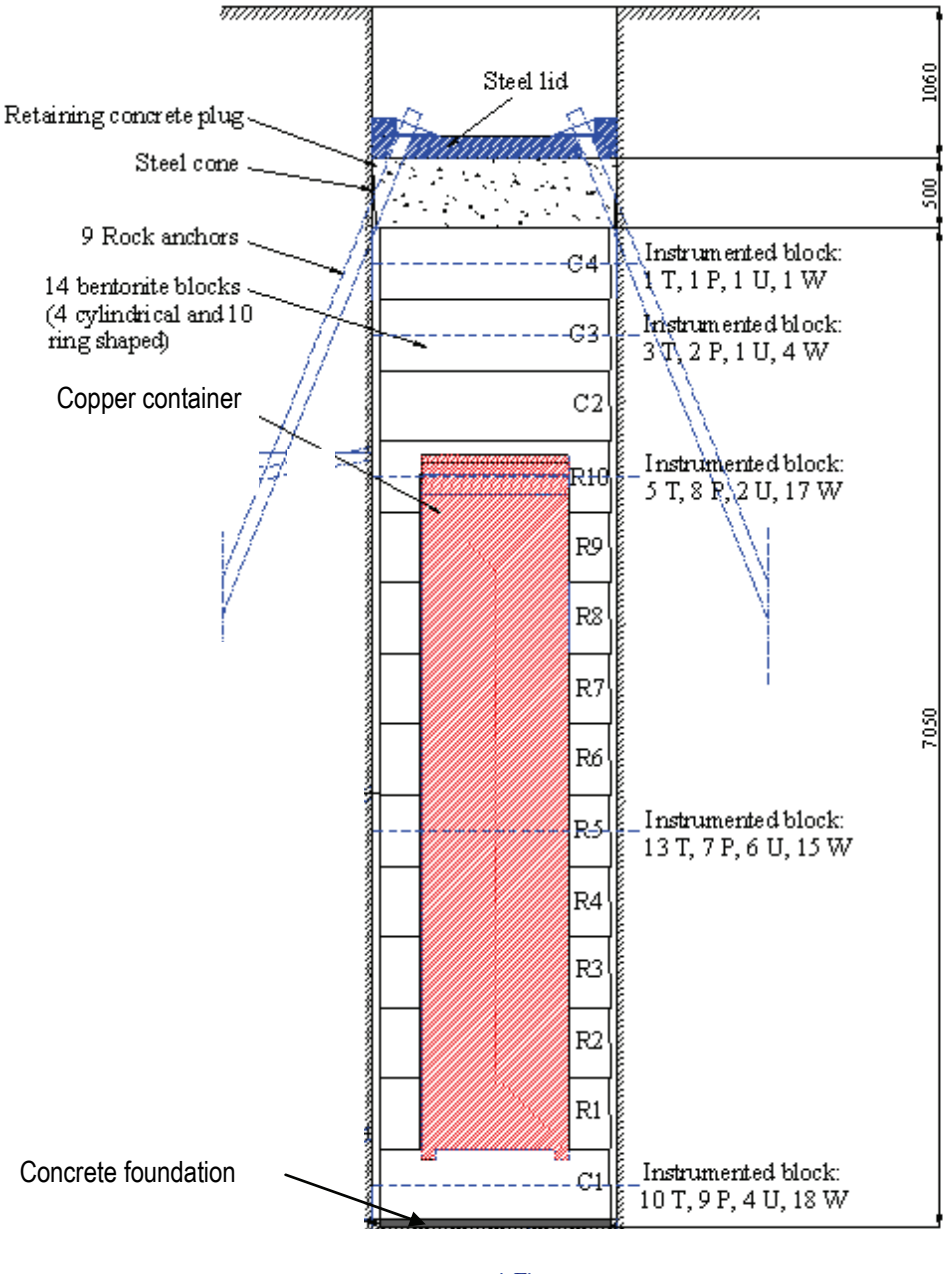

Figure 2: Schematic View Showing the Experiment Layout. Sensors have been placed in five of the bentonite blocks. For each block the number of each sensor type is described. (T=temperature, P=total pressure cell, U=pore pressure cell and W=relative humidity sensor)[2]

[2] O. Kristensson, L. Börgesson. CRT-canister retrieval test: EBS task force assignment.

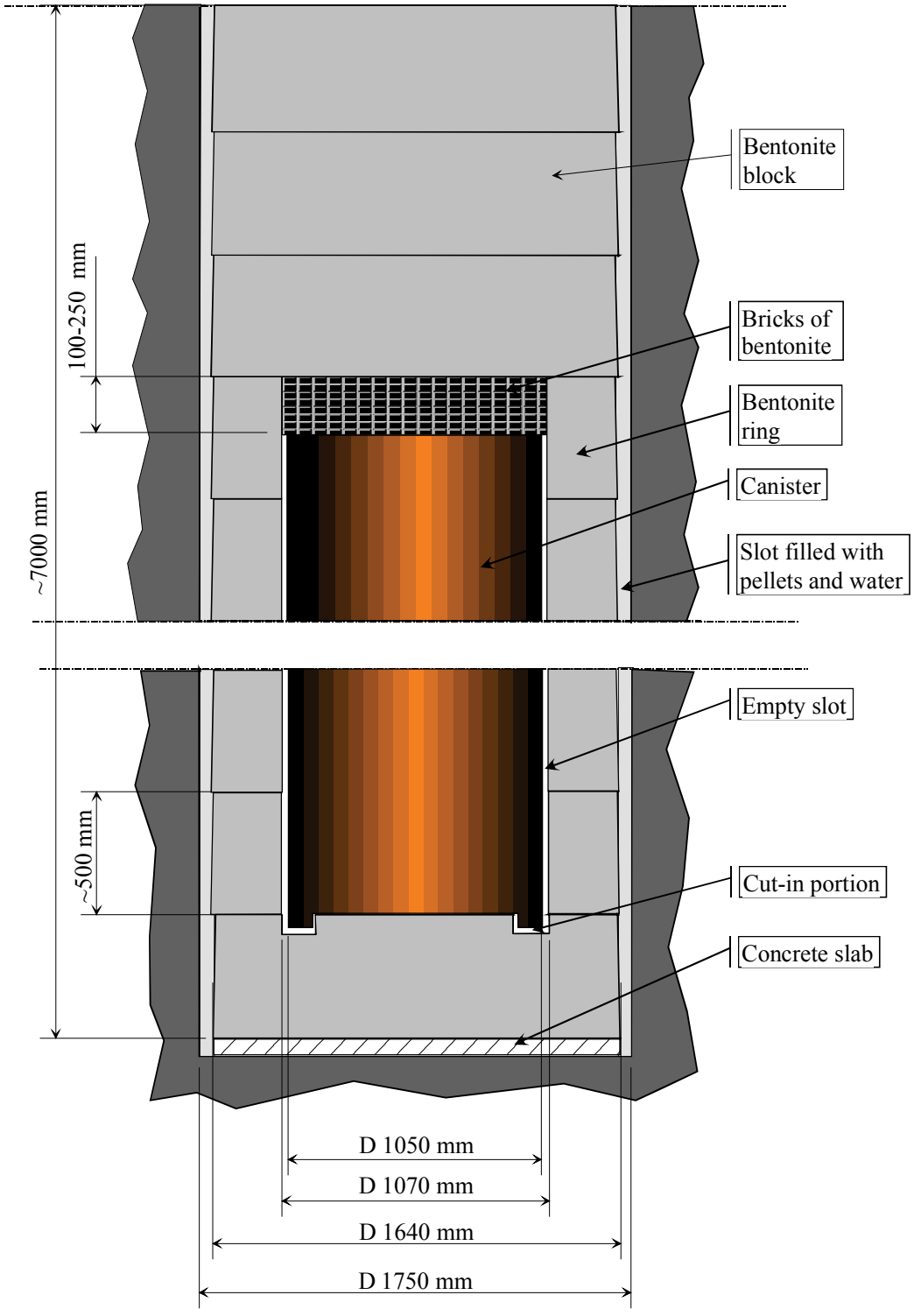

Figure 3: Schematic Drawing of the Container Hole with Bentonite Blocks with Dimensions in mm[3]

[3] O. Kristensson, L. Börgesson. CRT-canister retrieval test: EBS task force assignment.

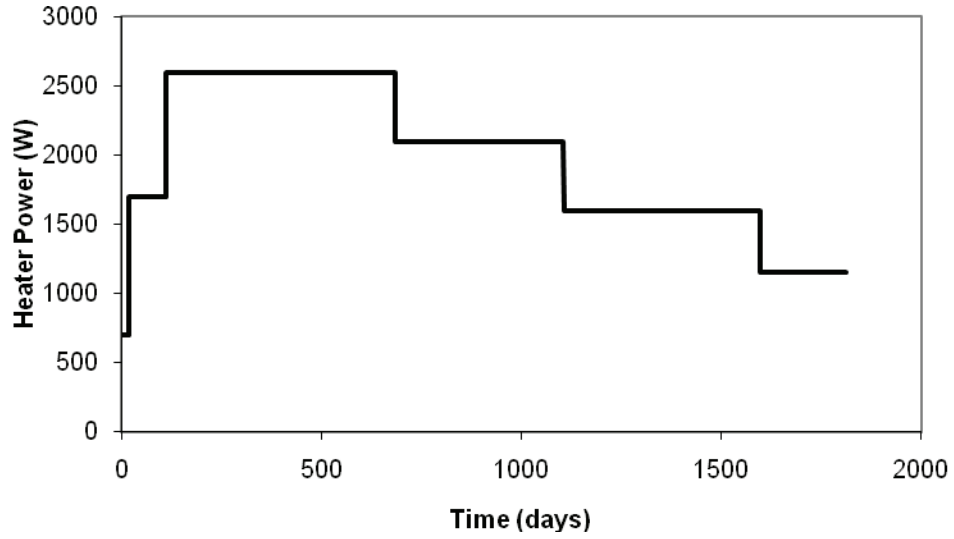

Figure 4: Container Power Protocol of the CRT

The water pressure in the filter mats was 0 kPa at the start of the experiment (October 23, 2000) and then stepwise increased to 0.8 MPa in the period of September 5 to October 10, 2002 (days 687-713). The detailed water pressure protocol is shown in Figure 5.

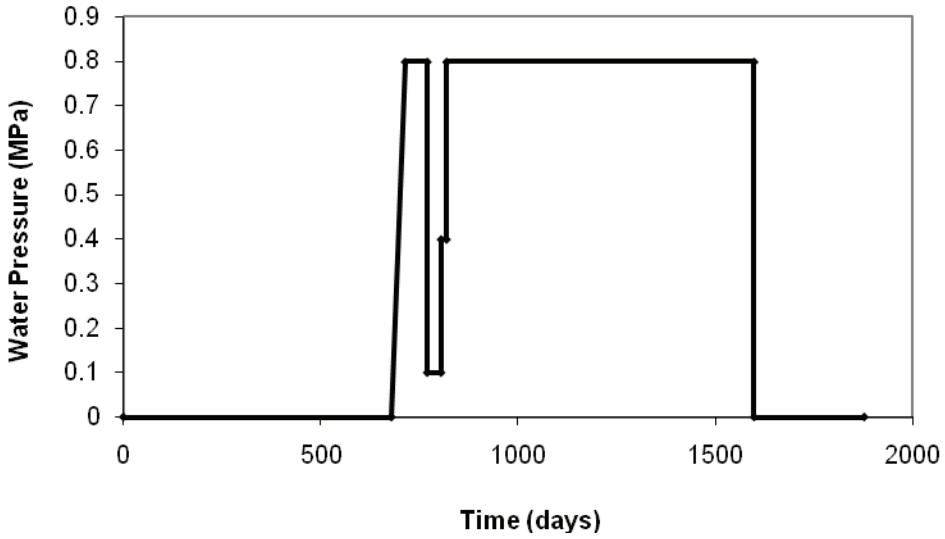

Figure 5: Filter Mat Pressure Protocol of the CRT

Figure 6 shows locations of some instruments in bentonite rings R5, R10, bentonite cylinder C3 and bentonite bricks. The Vaisala sensors W119, W120 and W121 measure the relative humidity (these sensors are also used to measure the temperature) in bentonite ring R5. The Vaisala sensors functioned very well when the relative humidity was below 96% and broke down after 600 days when temperature suddenly dropped. The Wescore sensors W122, W123 and W124 measured the suction in bentonite ring R5. They functioned well when relative

humidity was above 95%. The Geokon sensors P110, P111 and U106 were used to measure the vertical total pressures in bentonite Ring R5. The Geokon sensors P119 and P125 were used to measure the vertical total pressures in bentonite ring R10 and bentonite cylinder C3, respectively. The Vaisala sensor W134 was used to measure relative humidity in bentonite bricks and sensors W142 and W137 were used to measure suctions in bentonite ring R10. The Vaisala sensors W151 and W153 were used to measure the relative humidity in bentonite cylinder C3. The thermocouples T127 and T129 were used to measure the temperatures in bentonite R10 and bentonite cylinder C3, respectively.

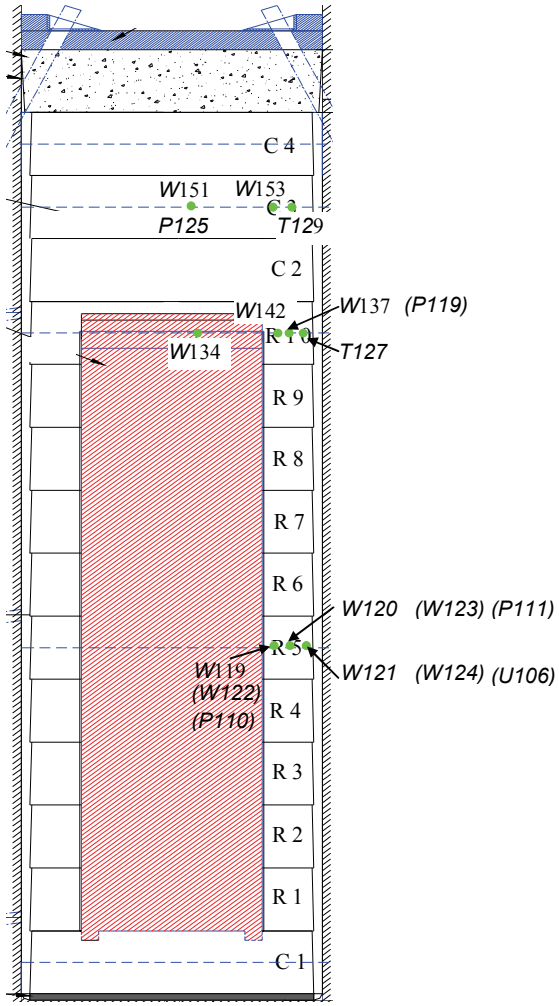

Figure 6: Locations of Measurement Instruments in the Bentonite Rings, Bentonite Bricks, and Bentonite Cylinders

3. GEOMETRIES, BOUNDARY CONDITIONS AND INITIAL CONDITIONS

The following modelling activities were done as part of this work.

- One-dimensional coupled thermal-hydraulic (TH)
- Two-dimensional coupled TH model
- One-dimensional coupled thermal-hydraulic-mechanical (THM) model
- Two-dimensional coupled THM model

3.1 ONE-DIMENSIONAL MODEL

3.1.1 Geometry for One-Dimensional Model

Bentonite ring R5 was simulated in a one-dimensional model. Figure 7 shows the geometry used for the one-dimensional model. There are three kinds of materials included in the one-dimensional model: the gap between the container and the bentonite ring, the bentonite ring and the pellets between the bentonite ring and the surrounding rock. It is an axisymmetrical one-dimensional model. The radius from the centre of the container to the inside surface of the gap is 0.525 m. The radius of the outer side surface of the model is 0.875 m. The vertical thickness of the model is 0.02 m. Figure 8 shows the mesh of the one-dimensional model. There are totally 50 elements and 102 nodes.

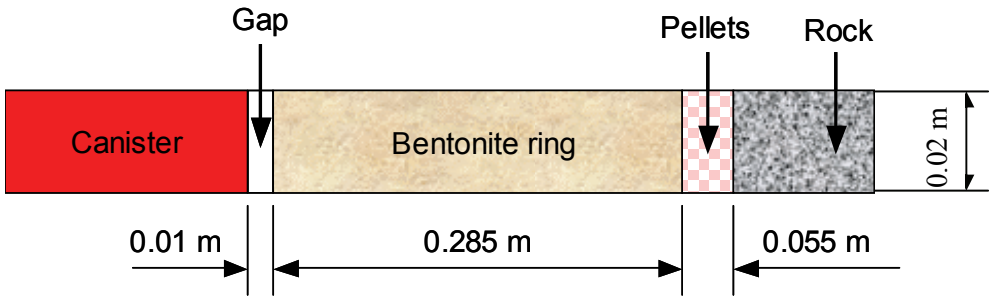

Figure 7: Geometry for One-Dimensional Model

3.1.2 Boundary Conditions and Initial Conditions for One-Dimensional Model

3.1.2.1 Boundary Conditions

Thermal Boundary Conditions:

- The temperatures at the nodes near the container were set at the temperature measured by sensor P12, which measured the temperature of the container surface, as shown in Figure 9;
- The temperatures at the borehole wall were set at temperatures measured by sensor TR125, which measured the temperatures on the wall of the borehole near mid-height of container, as shown in Figure 9; and
- There is no heat flux on the top and the bottom of the model.

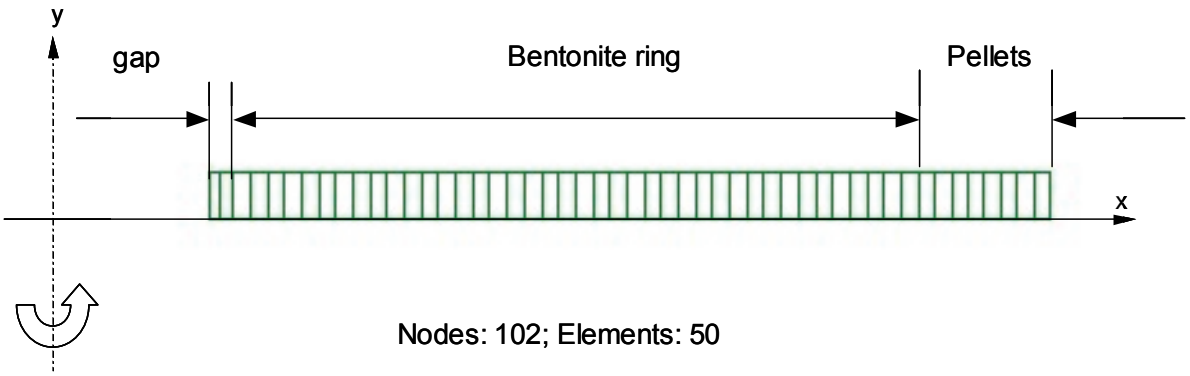

Figure 8: Mesh for One-Dimensional Model

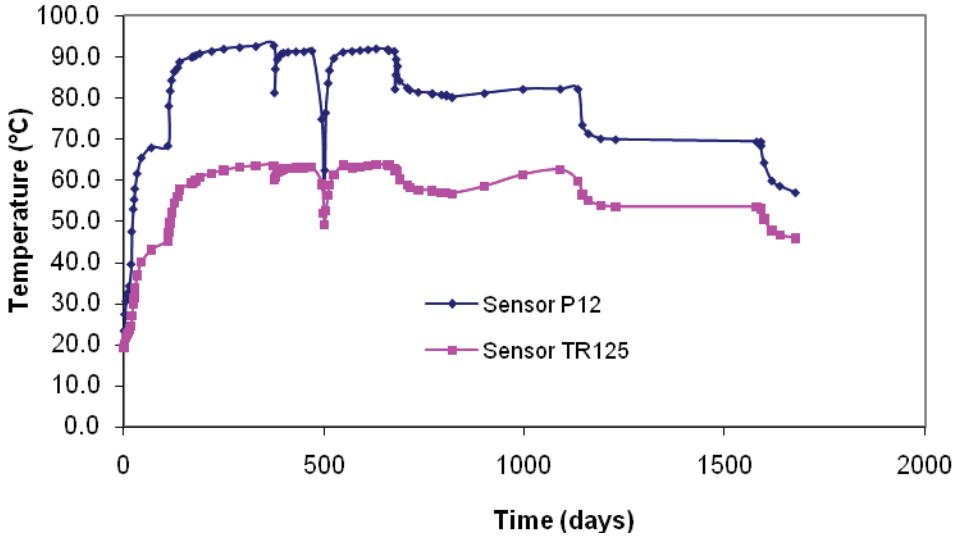

Figure 9: Measured Temperatures at Locations of Sensors P12 and TR125

Hydraulic Boundary Conditions:

- There is no water flux on the top, the bottom and the inner side boundary of the model; and
- The hydraulic head at the nodes of the bentonite pellets was fixed at the water pressure from the filter protocol as shown in Figure 5.

Mechanical Boundary Conditions:

- The nodes on the bottom and the top of the model were fixed in the vertical direction; and
- The nodes on the inside surface and the outside surface were fixed both in the vertical and horizontal directions.

3.1.2.2 Initial Conditions

Initial Thermal Conditions:

- Initial temperatures on all nodes were set at 20°C

Initial Hydraulic Conditions:

- Initial saturations of ring-shaped bentonite blocks and bentonite pellets were set at 0.859 and 0.895, respectively; and
- Initial saturation of gap was set at 1.0.

Initial Mechanical Conditions:

- Initial stress and initial displacement for all of nodes in the model were set at 0.

3.2 TWO-DIMENSIONAL MODEL

3.2.1 Geometry for Two-Dimensional Model

Figure 10 shows the geometry and the dimensions of the two-dimensional model. It is an axisymmetrical 2-D model. The radial dimension is 60 m from the axis of the borehole to the outer surface of the model. The distance from the top of the model to the roof of the tunnel is 50 m and the distance from the bottom of the model to the bottom of the borehole is also 50 m. The two-dimensional model includes 9 kinds of materials. They are rock, heater, bentonite pellets, bentonite bricks, ring-shaped bentonite blocks, cylindrical bentonite blocks, empty slot, concrete plug and steel lid.

3.2.2 Boundary Conditions and Initial Conditions for Two-Dimensional Model

3.2.2.1 Boundary Conditions

Thermal Boundary Conditions:

- The temperatures at the nodes on the tunnel surface and on the top of steel lid were set at 15°C.
- There is no heat flux at the nodes on the top, the axis of the model, the bottom and the outer vertical boundary.
- The heat flux was uniformly applied at the nodes of the container and the total heat flux was equal to the power protocols of the CRT as shown in Figure 4.

Hydraulic Boundary Conditions:

- There is no water flux on the top, the bottom and the outer vertical boundaries, the axis of the model, the tunnel surface and the top surface of steel lid.
- The hydraulic head at the nodes of bentonite pellets was fixed at the water pressure from filter pressure protocol as shown in Figure 5.

Mechanical Boundary Conditions:

- The nodes of the granite were fixed in both the vertical and the horizontal directions; and
- The nodes of the container heater were fixed in both the vertical and the horizontal directions.

3.2.2.2 Initial Conditions

Initial Thermal Conditions:

- Initial temperatures on all nodes were set at 20°C.

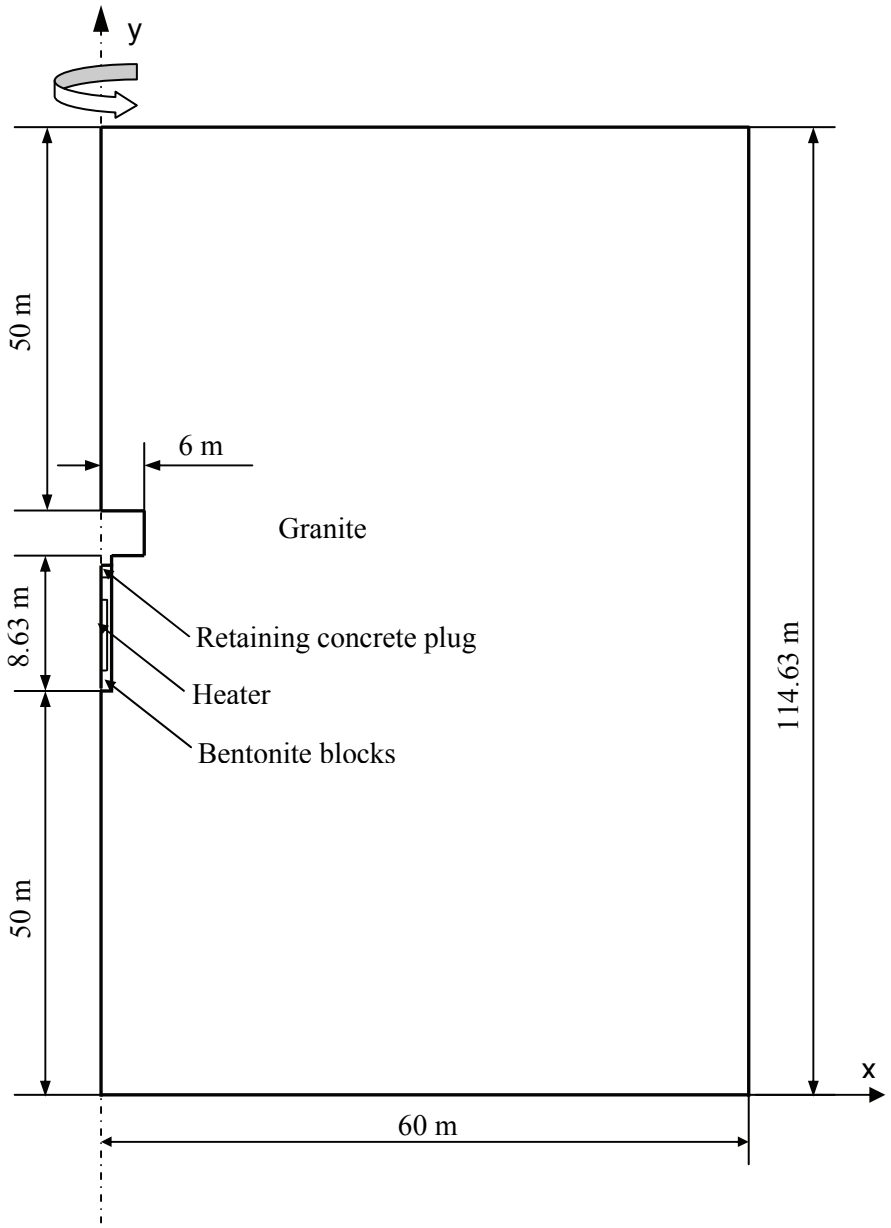

Figure 10: Dimensions of the Two-Dimensional Model

Initial Hydraulic Conditions:

- Initial saturations of cylinder-shaped bentonite blocks, ring-shaped bentonite blocks, bentonite pellets and bentonite bricks were set at 0.751, 0.859, 0.895 and 0.627, respectively.
- Initial saturation of gap was set at 1.0.
- Initial saturation of other materials was set at 0.*Initial Mechanical Conditions:*
- Initial displacements in the X-, Y- and Z-directions for all of nodes in the model were set at 0.
- Initial stresses were set at 0.5 MPa, 0.5 MPa and 0.5 MPa in the X-, Y- and Z-directions, respectively.

Figure 11 shows the mesh of the 2-D model. The rule of meshing is that the elements are small and dense near the heater becoming larger and less dense at greater distances from the heater. All of the elements are quadrangular. The total number of the elements and nodes are 2679 and 2803, respectively.

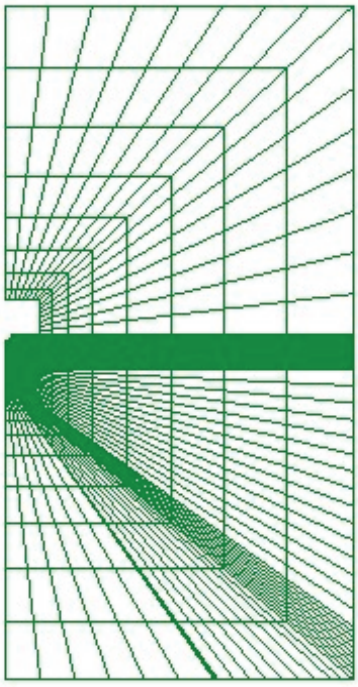

Nodes: 2803
Elements: 2679

There are 9 kinds of materials. They are rock, bentonite rings, bentonite bricks, bentonite cylinders, bentonite pellets, canister, gaps between canister and bentonite materials, concrete and steel lid.

Figure 11: Meshes of the Two-Dimensional Model

3.3 MATERIAL PARAMETERS

3.3.1 Hydraulic Parameters of Materials

Bentonite Materials:

For the solid blocks of highly compacted bentonite, the initial degree of saturation was 0.751, γ_d is the dry density, 1699 kg/m^3, void ratio was 0.636 and G_s is the specific gravity, 2.65 (Gatabin and Billaud 2005).

For the bentonite ring shaped blocks, the initial degree of saturation was 0.849, γ_d is the dry density, 1782 kg/m^3, void ratio was 0.56 and G_s is the specific gravity, 2.65 (Gatabin and Billaud 2005).

For the bentonite bricks, the initial degree of saturation was 0.637, γ_d is the dry density, 1616 kg/m^3, void ratio was 0.72 and G_s is the specific gravity, 2.65 (Gatabin and Billaud 2005).

For the bentonite pellets, the initial degree of saturation was 0.895, γ_d is the dry density, 1001 kg/m^3, void ratio was 1.778 and G_s is the specific gravity, 2.65 (Gatabin and Billaud 2005).

The relation between saturation and suction using the CODE_BRIGHT manual suggested equation is as follows:

$$S_{re} = \left[1 + \left(\frac{s}{P_0}\right)^{1/(1-\beta_1)} \right]^{-\beta_1} \quad (1)$$

where s is suction, MPa; P_0 is an estimated parameter; β_1 is an estimated parameter. Based on the measurements in Hokmark and Falth (2003), Dang and Robinet (2004) and Villar (2003), the values of P_0 and β_1 were selected as follows: for the bentonite solid blocks, the bentonite ring shaped blocks and the bentonite bricks, P_0 = 40.0, β_1 =0.4; for the bentonite pellets, P_0 = 10.0, β_1 =0.6. S_{re} is the effective degree of saturation, taking into account that not all water is removed during oven drying of buffer at a temperature of 110°C, as follows:

$$S_{re} = \frac{S_r - S_{rres}}{S_{r\max} - S_{rres}} \quad (2)$$

where S_r is the absolute degree of saturation, S_{rres} is the degree of residual saturation representing the remaining mass of retained water at a temperature of 110°C (i.e., 0.05) and S_{rmax} is the degree of maximum saturation (i.e., 1.0).

For the cylindrical bentonite blocks, their saturated hydraulic conductivity was assumed to be 2.1x10^{-14} m/s (Borgesson and Hernelind 1999). For the bentonite ring shaped blocks and bentonite bricks, their saturated hydraulic conductivity was assumed to be 0.8x10^{-14} m/s. For the bentonite pellets, their saturated hydraulic conductivity was assumed to be 0.8x10^{-11} m/s.

The relative permeability of the liquid phase ($k_{rl} = S_{re}^{4}$) was adopted for all of bentonite materials. Relative permeability is the ratio of the permeability at a certain degree of saturation to the permeability at maximum saturation.

Rock, Steel, Concrete and Heater:

The rock, steel, concrete and heater steel shell were treated as impermeable and were assigned a 6 orders of magnitude lower hydraulic conductivity than the clay and a retention curve using Equation (1) with P_0=1 x 10^{-6} and β_1 = 0.5.

3.3.2 Thermal Parameters of Materials

The following expression of the variation of bentonite thermal conductivity with saturation was used in this calculation.

$$\lambda = \lambda_{sat}^{S_l} \lambda_{dry}^{(1-S_l)} \tag{3}$$

in which λ_{sat} is the saturated thermal conductivity of the clay and λ_{dry} is the dry thermal conductivity of the clay. Based on the measured information in Börgesson et al. (1995), the values of λ_{sat} and λ_{dry} for bentonite solid blocks, bentonite ring shaped blocks and bentonite bricks were selected to be 1.3 W/(m·K) and 0.3 W/(m·K), respectively. The values of λ_{sat} and λ_{dry} for bentonite pellets were selected to be 1.3 W/(m·K) and 0.17 W/(m·K). The specific heat of the bentonite materials was set at 800 J/(kg·K).

The thermal conductivity of the rock, the steel shell, the concrete and heater were set to 2.51 W/(m·K), 50 W/(m·K), 2.7 W/(m·K) and 300 W/(m·K), respectively. The specific heats of the rock, the steel shell, the concrete and the heater were set at 770 J/(kg·K), 460 J/(kg·K), 770 J/(kg·K) and 460 J/(kg·K), respectively.

3.3.3 Mechanical Parameters of Materials

The Basic Barcelona elasto-plastic model (BBM) developed by Alonso et al. (1990) was applied for the cylindrical bentonite blocks, ring-shaped bentonite blocks and bentonite bricks. The incremental volumetric elastic strain $d\varepsilon_v^e$ is calculated using the following equation:

$$d\varepsilon_v^e = (\frac{k}{1+e})(\frac{dp'}{p'}) + (\frac{k_s}{1+e})(\frac{ds}{s+0.1}) + \alpha_0 dT \tag{4}$$

where e is void ratio; $p' = \frac{1}{3}(\sigma_x + \sigma_y + \sigma_z) - \max(p_g, p_l)$; k_s is a dimensionless compressibility coefficient under suction changes (ds) for each associated suction (s); k is a dimensionless compressibility coefficient under mean stress changes; α_0 is volumetric thermal expansion, $°C^{-1}$.

The plastic strain can be obtained by plasticity theory. The equation for the yield curve in the (p, s) space is:

$$\left(\frac{p_0}{p^c}\right)=\left(\frac{p_0^*}{p^c}\right)^{[\chi(0)-k]/[\chi(s)-k]} \tag{5}$$

where p_0^* is the preconsolidation stress for saturated conditions; p^c is a reference stress; $\chi(s)$ is the stiffness parameter that is a function of suction as shown in Equation (5).

$$\chi(s)=\chi(0)\left[(1-r)\exp(-\beta\cdot s)+r\right] \tag{6}$$

where $\chi(0)$ is the stiffness parameter at saturation; r is a parameter defining the maximum soil stiffness; s is suction and β is a constant describing the rate of increase in soil stiffness with suction.

The parameters used in the coupled THM modelling for cylindrical bentonite blocks, ring-shaped bentonite blocks and bentonite bricks are shown in Table 1.

Table 1: Mechanical Parameters used for Bentonite Materials in Coupled THM Modelling

	Cylindrical Bentonite Blocks	Ring-shaped Bentonite Blocks	Bentonite Bricks
P^*_0 (MPa)	0.359	0.359	0.359
$\chi(0)$	0.621	0.621	0.621
κ	0.28	0.28	0.28
r	0.75	0.75	0.75
β (MPa^{-1})	0.05	0.05	0.05
p^c (MPa)	0.18	0.18	0.18
k_s	0.04	0.04	0.04
υ	0.2	0.2	0.2
G (MPa)	24	24	24
M	0.526	0.526	0.526
α_0 ($°C^{-1}$)	$3x10^{-5}$	$3x10^{-5}$	$3x10^{-5}$

The concrete plug, steel lid and bentonite pellets were assumed to be linear elastic materials. Their mechanical parameters are shown in Table 2.

Table 2: Mechanical Parameters used for Concrete Plug, Steel Lid and Bentonite Pellets

	Concrete Plug	Steel Lid	Bentonite Pellets	Empty Gap
Young's modulus, E, (MPa)	30,000	200,000	3	3
Poisson's ratio, υ	0.2	0.2	0.2	0.2
Linear thermal expansion, α, ($°C^{-1}$)	$9.8x10^{-5}$	$1.6x10^{-5}$	$1x10^{-5}$	0

4. MODELLING RESULTS AND COMPARISON WITH MEASUREMENTS

4.1 MODELLING RESULTS FROM ONE-DIMENSIONAL MODEL AND COMPARISON WITH MEASUREMENTS

4.1.1 Temperatures

4.1.1.1 Simulated Temperatures

Figures 12 and 13 show the simulated temperatures at different locations along bentonite R5. For different locations, they follow the same pattern as shown in Figure 4. The further the nodes are from the axis of the borehole, the lower the temperatures.

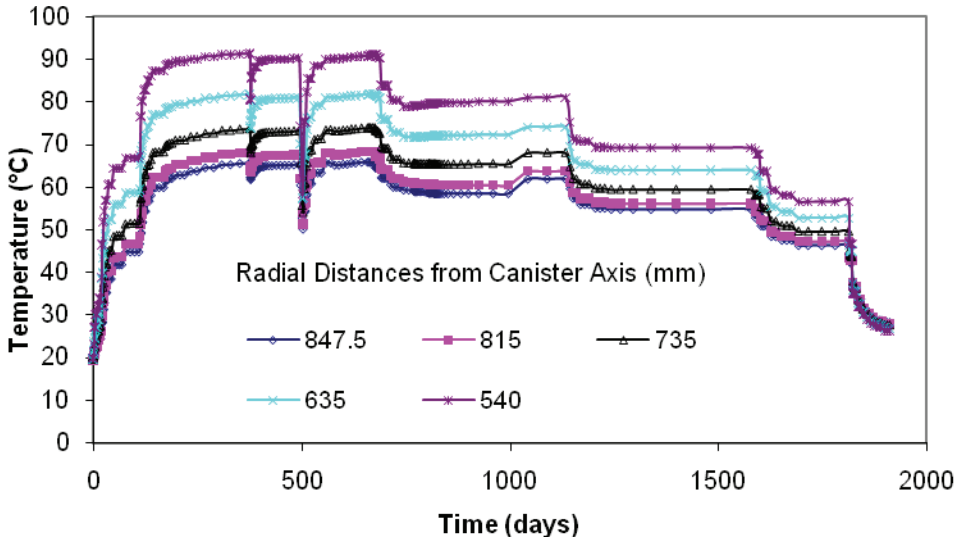

Figure 12: Simulated Temperatures at Locations with Radial Distances of 540 mm, 635 mm, 735 mm, 815 mm and 847.5 mm from the Container Axis

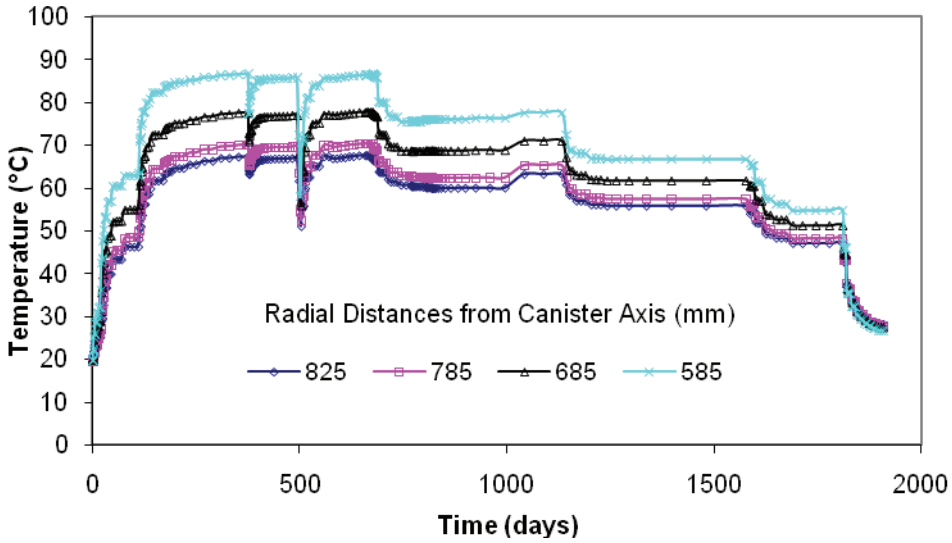

Figure 13: Simulated Temperature at Locations with Radial Distances of 585 mm, 685 mm, 785 mm and 825 mm from the Container Axis

Figure 14 shows the temperature against the distance from the axis of the heater along bentonite ring R5 at four different times. The temperatures decreased almost linearly with distance from the heater surface from a maximum of 92.4 °C to 63.7°C by Day 670. However, the temperatures are 26.3°C on the heater surface and 28.5°C on the borehole surface at the end of the test.

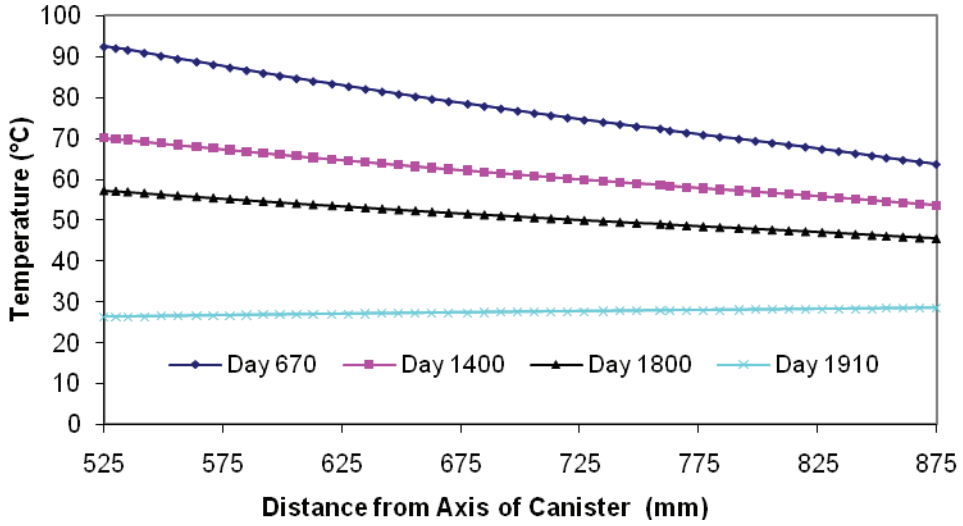

Figure 14: Profiles of Simulated Temperatures at Times of Day 670, Day 1400, Day 1800 and Day 1910

Figure 15 shows the simulated temperature contours in the empty gap, bentonite ring and bentonite pellets at four different times. On Day 110, the temperatures are from 68°C to 43°C from the heater surface to the borehole surface. On Day 670, the temperatures increased to 92°C on the heater surface and 64°C on the borehole surface. On Day 1400, the temperatures dropped to 70°C on the heater surface and 54°C on the borehole surface. On Day 1800, the temperatures continued dropping to 57°C on the heater surface 46°C from the heater surface and on the borehole surface.

4.1.1.2 Comparison of Temperatures between Simulations and Measurements

Figure 16 shows the comparison of the simulated and the measured temperatures at three different locations of T111, T121 and T112. T111, T121 and T112 are 0.635 m, 0.685 m and 0.735 m from the container axis in bentonite ring R5, respectively. At these three different locations, the simulated results matched the measured temperatures very well. Figure 17 shows the comparison of temperatures between simulated results and measurements at locations of sensors W119, W120 and W121. The simulated temperatures matched the measurement at three different locations very well during the first 600 days. After about 600 days, Vaisala sensors W119, W120 and W121 broke down.

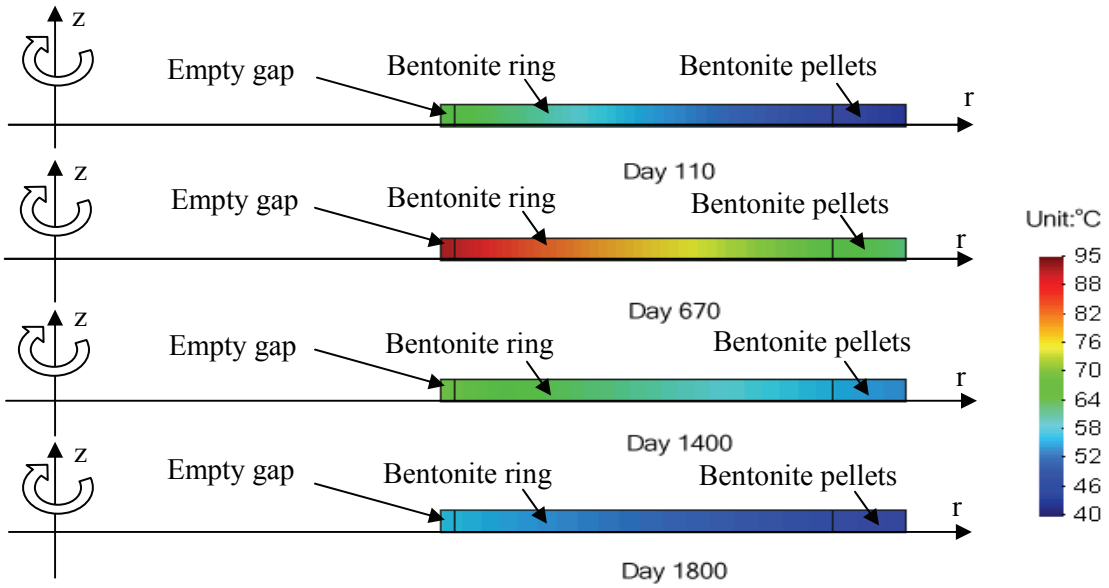

Figure 15: Simulated Temperature Contours in the Empty Gap, Bentonite Ring and Bentonite Pellets at Four Different Times

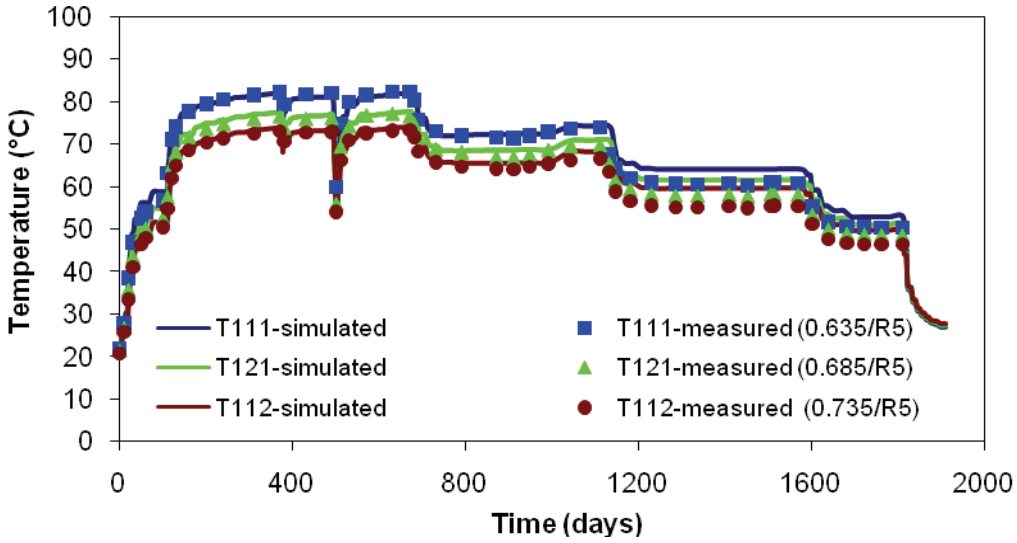

Figure 16: Comparison of Temperatures between Simulated Results and Measurements at Sensors of T111, T121 and T112

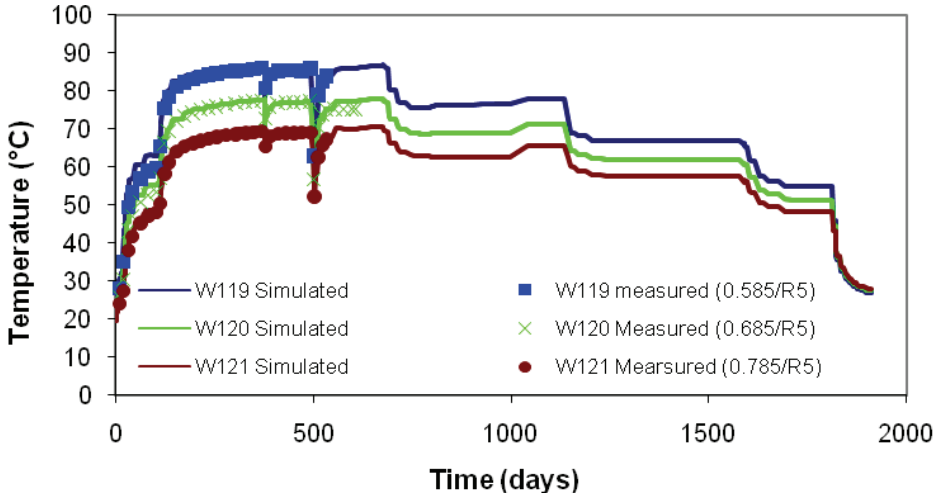

Figure 17: Comparison of Temperatures between Simulated Results and Measurements during the First 600 Days and Predicted Temperatures after 600 Days at Sensors of W119, W120 and W121

4.1.2 Hydraulic Response

4.1.2.1 Simulated Hydraulic Response in the Bentonite Materials

Figures 18 and 19 show the simulated water saturations at different locations along bentonite ring R5. At Day 1,000, the bentonite blocks were fully saturated.

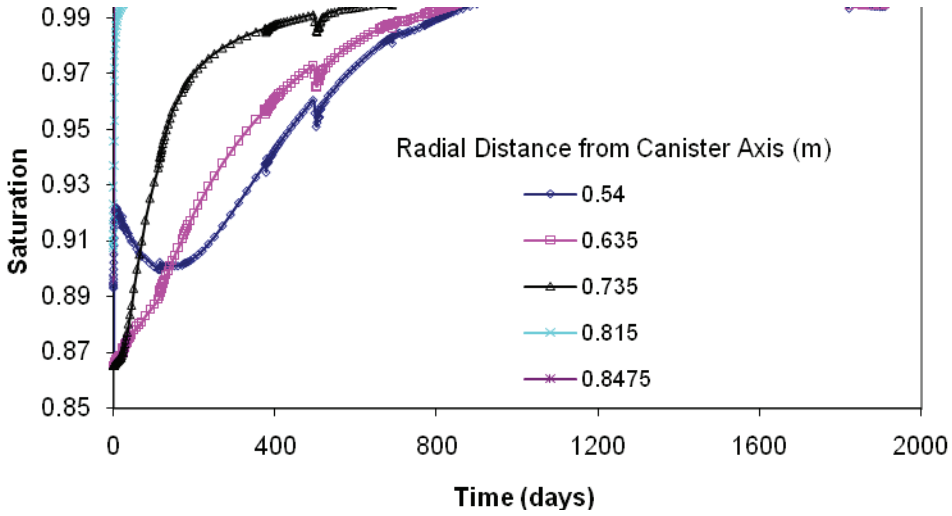

Figure 18: Simulated Water Saturations at Locations with Radial Distances of 540 mm, 635 mm, 735 mm, 815 mm and 847.5 mm from the Container Axis

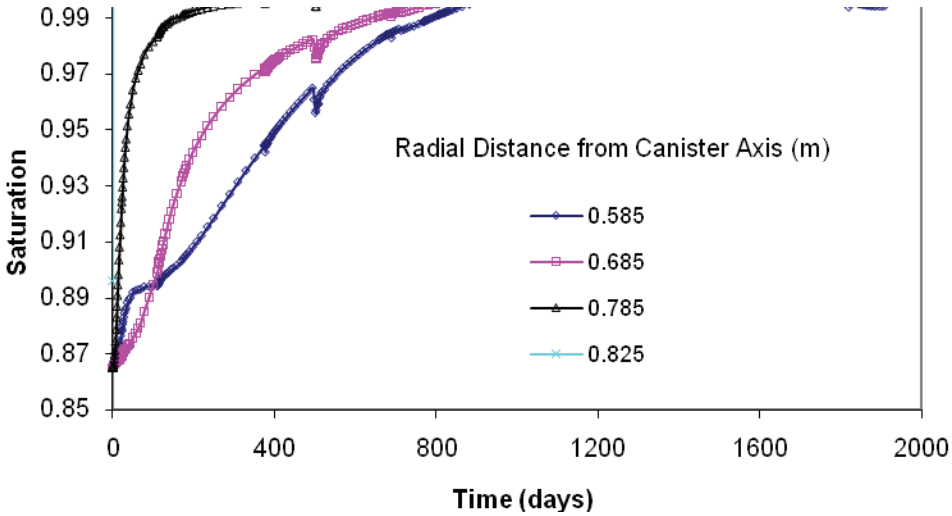

Figure 19: Simulated Water Saturation Histories at Locations with Radial Distances of 585 mm, 685 mm, 785 mm and 825 mm from the Container Axis

Figure 20 shows the simulated degree of saturation in the unfilled annular gap on level of R5. Its initial pore water pressure was assumed to be 0 MPa, meaning it was filled with water. Due to the suction provided by the ring-shaped bentonite and its expansion due to water uptake, the water originally in the empty gap was absorbed by ring-shaped bentonite blocks and the empty gap became unsaturated and was filled due to expansion of ring-shaped bentonite. When pressurized water was injected into pellets, the saturation of the bentonite in the originally empty gap increased and final became fully saturated. However, when the injected water pressure dropped to 0 MPa on Day 1598, the empty gap (ring-shaped bentonite block near the heater surface) became unsaturated again because of the heating.

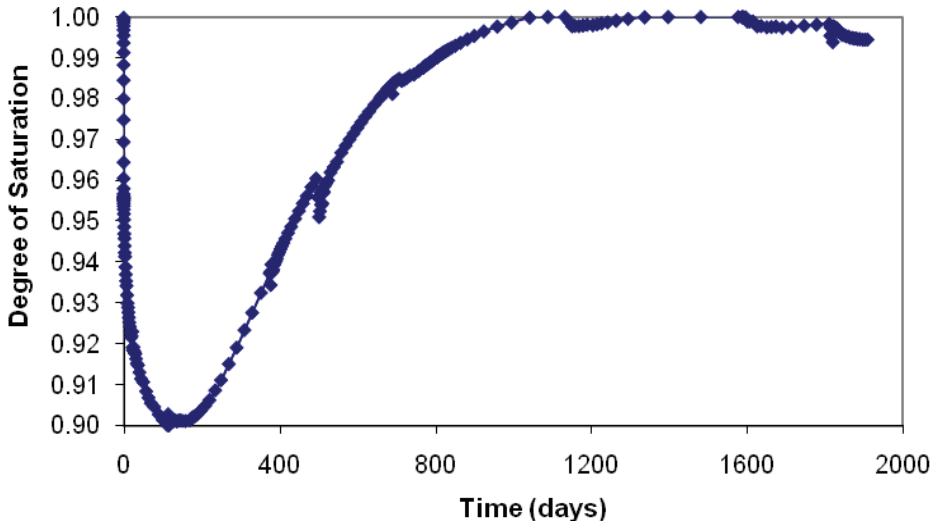

Figure 20: **Simulated Degree of Saturation in the Unfilled Annular Gap**

Figure 21 shows the simulated pore water pressure contours in the empty gap, bentonite ring and bentonite pellets at four different times. On Day 110, the suctions were from 22 MPa on the end near the heater to 0 MPa in the pellets. On Day 670, the suction decreased to 6.5 MPa on the end near the heater and 0 MPa in the pellets. On Day 1400, the pore water pressure was 0.4 MPa at the end near heater and 0.8 MPa in the pellets, indicating that all of the materials in Level R5 were fully saturated due to pressure water being injected. On Day 1800, the suction at the end near heater decreased to 1.5 MPa due to drying by heating and the pore water pressure in the pellets was back to 0 MPa.

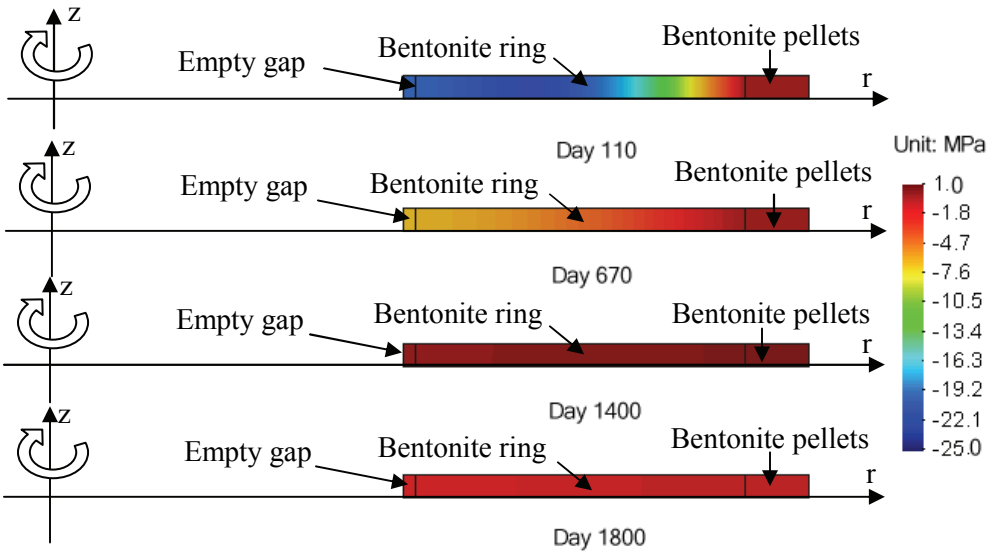

Figure 21: **Simulated Pore Water Pressures in the Empty Gap, Bentonite Ring and Bentonite Pellets at Four Different Times**

4.1.2.2 Comparisons of Simulated Hydraulic Response with Measurements

Figure 22 shows the comparison of the simulated relative humidity with measurements at locations of W119, W120 and W121. W119, W120 and W121 are 0.585 m, 0.685 m and 0.785 m from the container axis in bentonite ring R5, respectively (refer to Figure 6 for locations). The simulated relative humidity at locations of W121 and W120 matched the measurement very well. The simulated relative humidity at location of W119 was higher than the measurement for the first 270 days. After day 270 until 600 days, the simulated matched the measurement very well. After about 600 days, Vaisala sensors W119, W120 and W121 broke down.

Figure 23 shows the comparison of the simulated suctions with measurements at locations of W122, W123 and W124. W122, W123 and W124 are 0.585 m, 0.685 m and 0.785 m from the container axis in bentonite ring R5, respectively (refer to Figure 6 for locations). The simulated suction at location of W124 matched the measurements reasonably well. For locations of W122 and W123, the simulated suctions captured the main pattern of the measurements, but there were some differences in value.

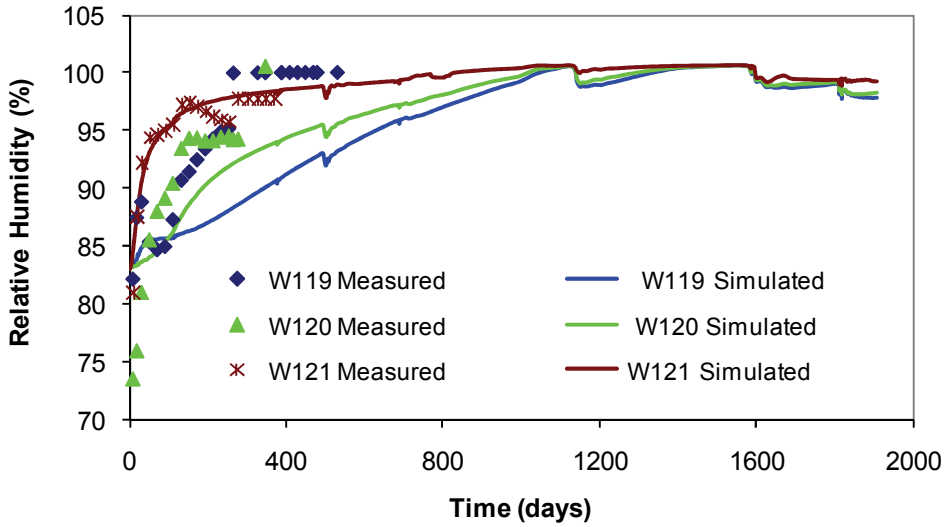

Figure 22: Comparison of Simulated Relative Humidity with Measurements during the First 600 Days and Predicted Relative Humidities after 600 Days at Locations of W119, W120 and W121

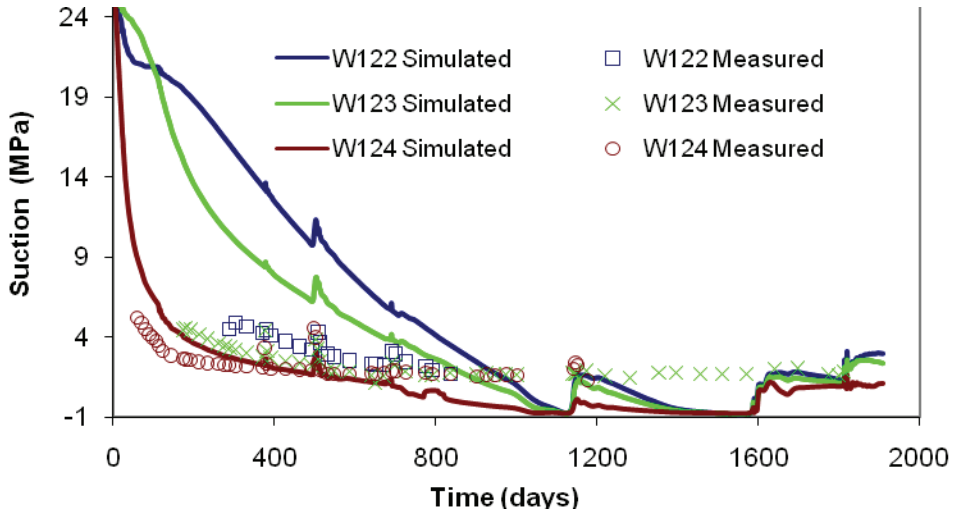

Figure 23: Comparison of Simulated Suctions with Measurements at Locations of W122, W123 and W124

4.1.3 Mechanical Response

Figure 24 shows the calculated vertical stress against time at different locations. The simulated results show that the range of vertical stress is from 0 MPa to 3.1 MPa. Figure 25 compares the simulated vertical stresses and measurements at three different locations of P110, P111 and U106. P110, P111 and U106 are located at 0.585 m, 0.685 m and 0.785 m from the container axis of the bentonite ring R5 (refer to Figure 6 for locations). The simulated vertical stress at location of U106 matched the measurement reasonably well not only in pattern but also in value. However, for locations of P110 and P111, the simulated results were much lower than the measurements.

4.1.4 Summary of the Results from One-Dimensional Modelling

The simulated temperatures at different location in ring-shaped bentonite R5 matched the measurements very well, indicating the thermal parameters used in this modelling for the empty gap, ring-shaped bentonite blocks and bentonite pellets were suitable and the thermal boundary conditions were correct.

The pattern of the simulated suctions in different locations in the ring-shaped bentonite blocks matched that of the measured suction reasonably well. The thermally induced relative humidity in the ring-shaped bentonite blocks captured the main characteristics of the relative humidity, but there were differences in the magnitudes of the suctions.

The simulated vertical stresses caught some main features of the measurements. However, the differences in value were obvious, indicating that the parameters used for the coupled THM modelling needed to be refined, or there is some as-yet unidentified feature or process that the model is not capturing accurately.

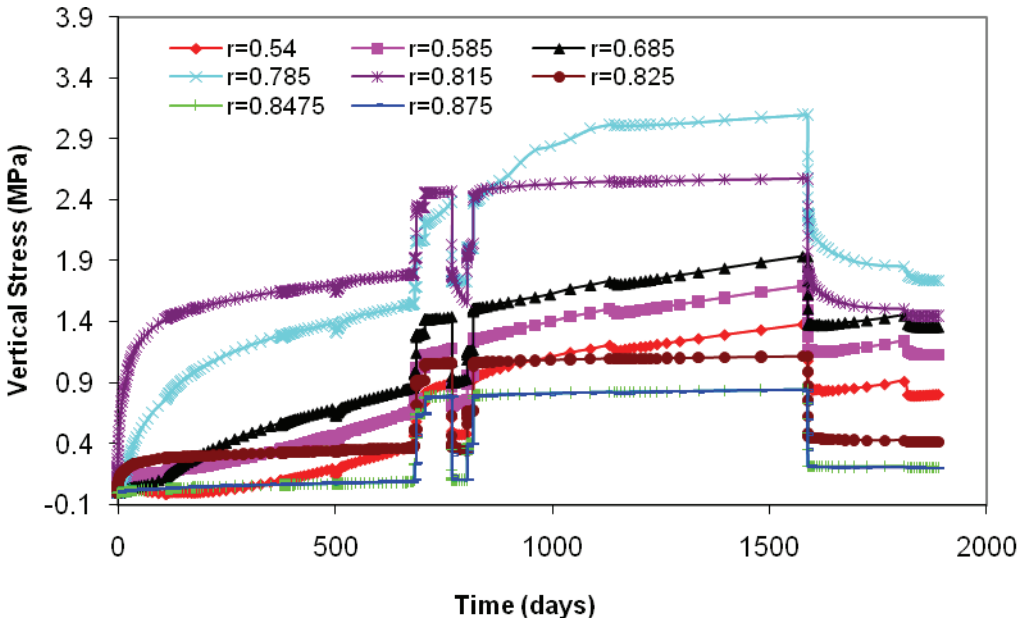

Figure 24: Simulated Vertical Stresses vs. Time at Different Locations

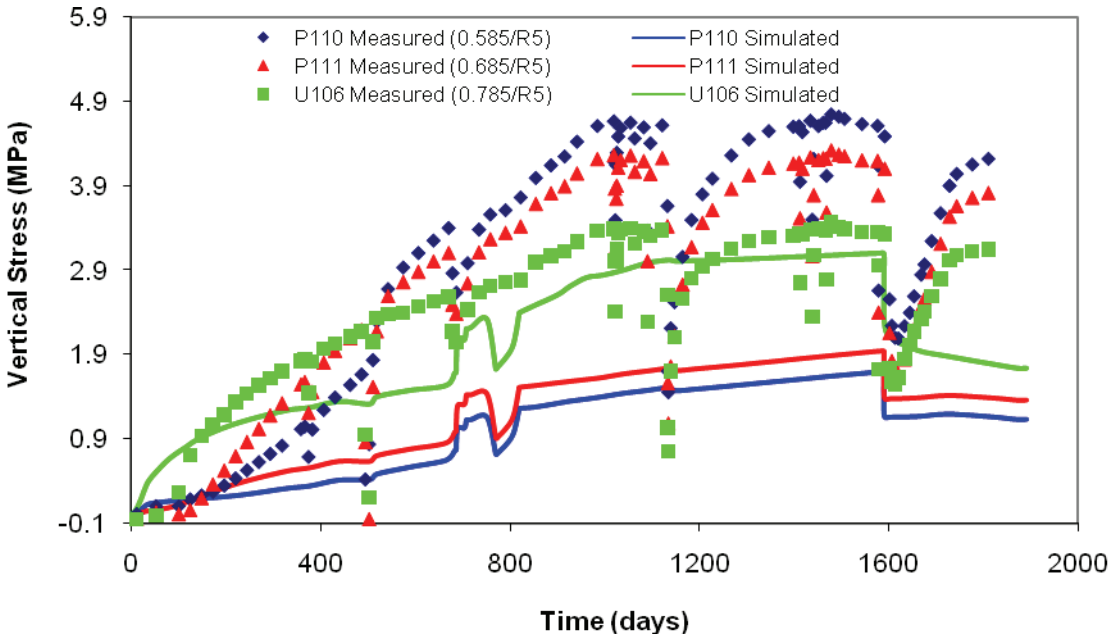

Figure 25: Comparison of Simulated Vertical Stresses and Measurements at Locations of P110, P111 and U106

4.2 MODELLING RESULTS FROM TWO-DIMENSIONAL MODEL AND COMPARISON WITH MEASUREMENTS

4.2.1 Thermal Response

4.2.1.1 Simulated Thermal Response in the Bentonite Materials

Figure 26 shows the simulated temperatures at different locations along a horizontal line in cylindrical bentonite block C3 (refer to Figure 2 for locations). At different locations, the temperatures show the similar pattern as shown in Figure 9. However, the value of their temperature is much smaller compared to the temperature near the heater. The highest temperature at location 0.05 m from the container axis was 37.5°C happening on Day 684. Figure 27 shows the profiles of temperatures at four different times on level C3. The temperature distributions at the four different times are very uniform.

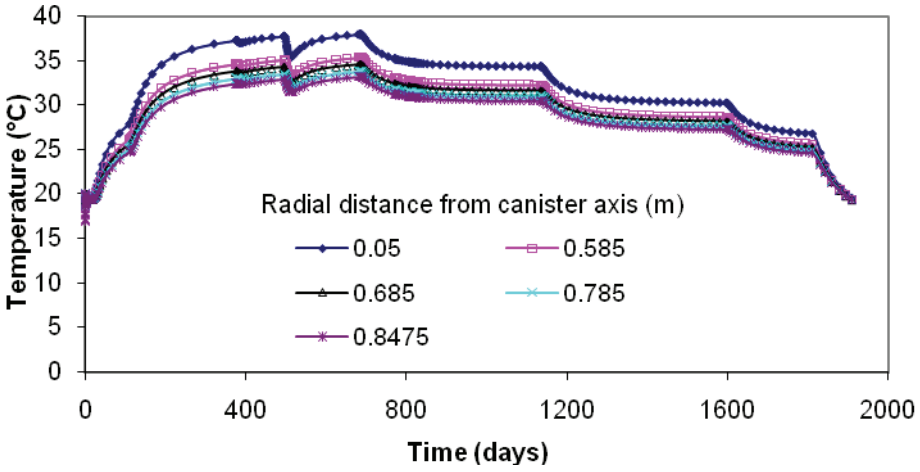

Figure 26: Simulated Temperatures at Different Radial Distances along Level C3

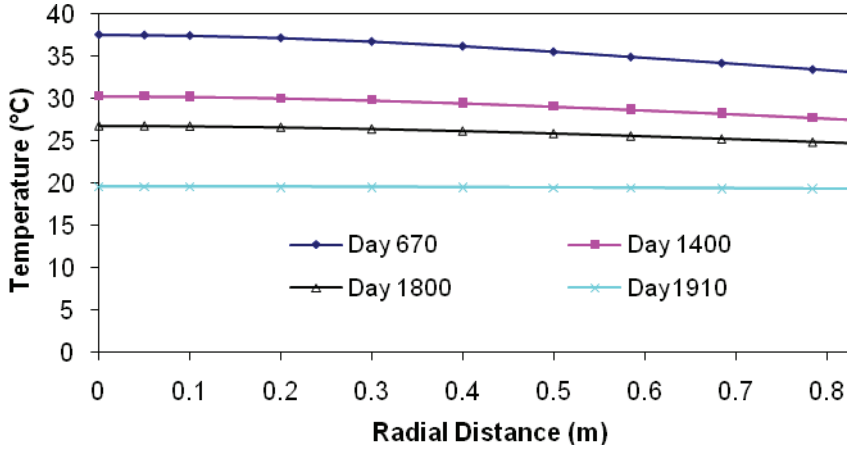

Figure 27: Profiles of Simulated Temperatures at Four Different Times along Level C3

Figure 28 shows the temperatures at different locations on level R10 (refer to Figure 2 for locations). They show the same pattern as those shown in level C3. However, the temperature value is much higher than those in level C3 because R10 was closer to the container than C3. The highest temperature was 81°C at location 0.05 m from container axis happening on Day 494 and 684.

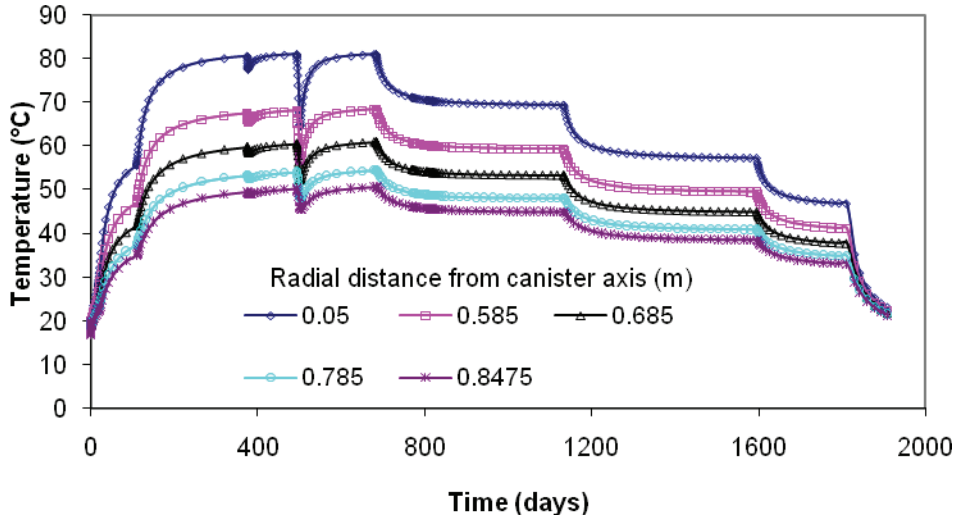

Figure 28: Simulated Temperatures at Different Radial Distances along Level R10

Figure 29 shows the simulated temperature profiles along level R10 at four different times of Day 670, 1400, 1800 and 1900. The temperatures are very uniform in the range of radial distance from container axis less than 0.4 m because it was located in bentonite bricks on the top of the heater. The temperature was 81°C at the centre of bentonite bricks and 49°C near the borehole surface on Day 670.

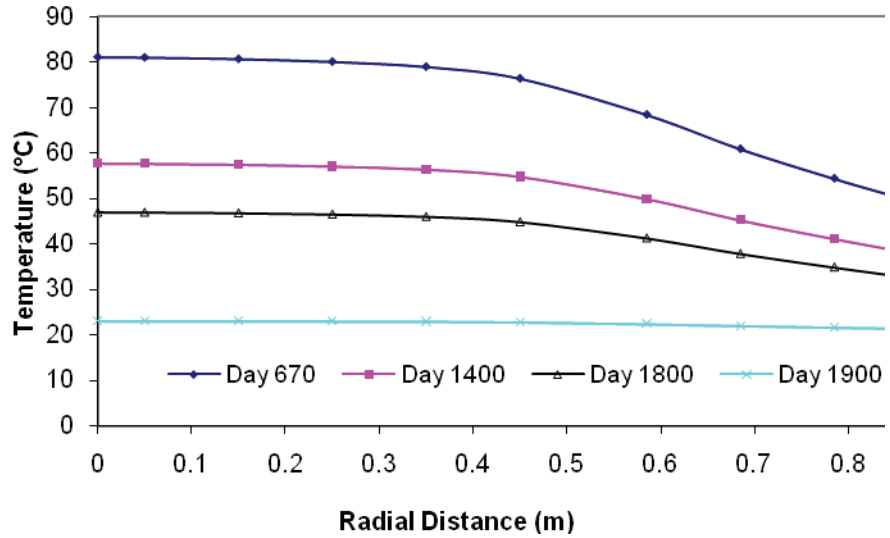

Figure 29: Simulated Temperature Profiles along Level R10 at Four Different Times

Figure 30 shows temperature histories at nine different locations on level R5. The temperatures at nine different locations show the same pattern as shown in Figures 9, 22 and 24. The highest temperature was 89°C occurring on Day 494 at location 0.54 m from the container axis.

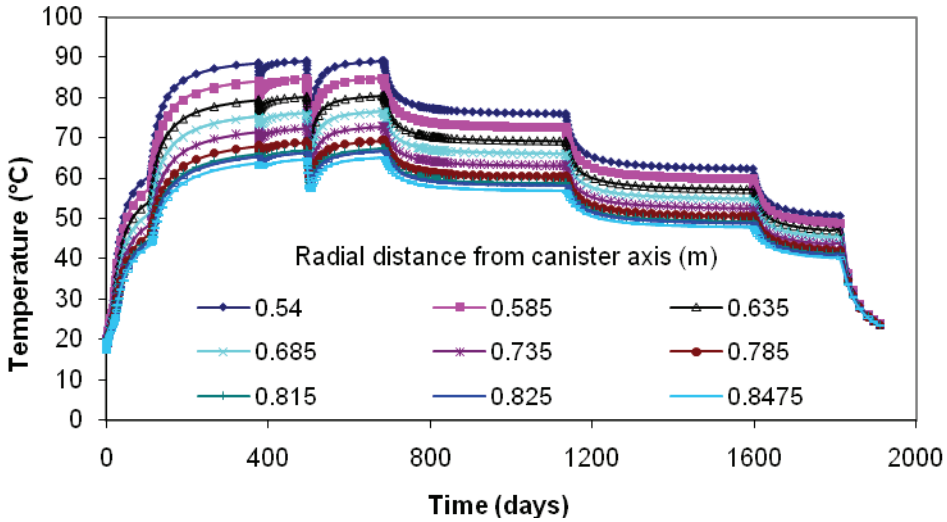

Figure 30: Simulated Temperature Histories at Different Radial Distances along Level R5

Figure 31 shows the temperature distributions along level R5 at four different times of Day 670, 1400, 1800 and 1910. They were almost linearly decreased from the location near heater to the location near borehole surface. The temperature varied from 91°C on the heater surface to 63°C on the borehole surface on Day 670.

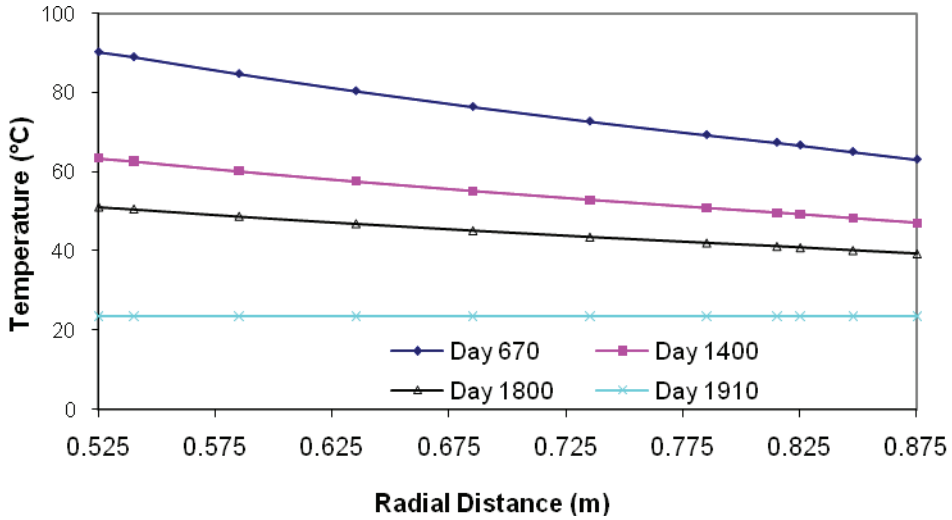

Figure 31: Profiles of Simulated Temperatures along Level R5 at Four Different Times

Figure 32 shows the temperature contours in the ring-shaped bentonite ring, bentonite pellets, bentonite bricks and cylindrical bentonite at four different times. On Day 110, the highest temperature around the heater (on the inside surface of the ring-shaped bentonite blocks, the bottom of bentonite bricks and on the top surface of cylindrical bentonite block below the heater) was 62°C and the lowest temperature near the bottom of the concrete plug was 17°C. On Day 670, the highest and lowest temperatures were 91°C and 19°C, respectively. Due to the decrease of heating power, the highest and lowest temperature decreased to 64°C and 18°C on Day 1400 and 51°C and 17.5°C on Day 1800.

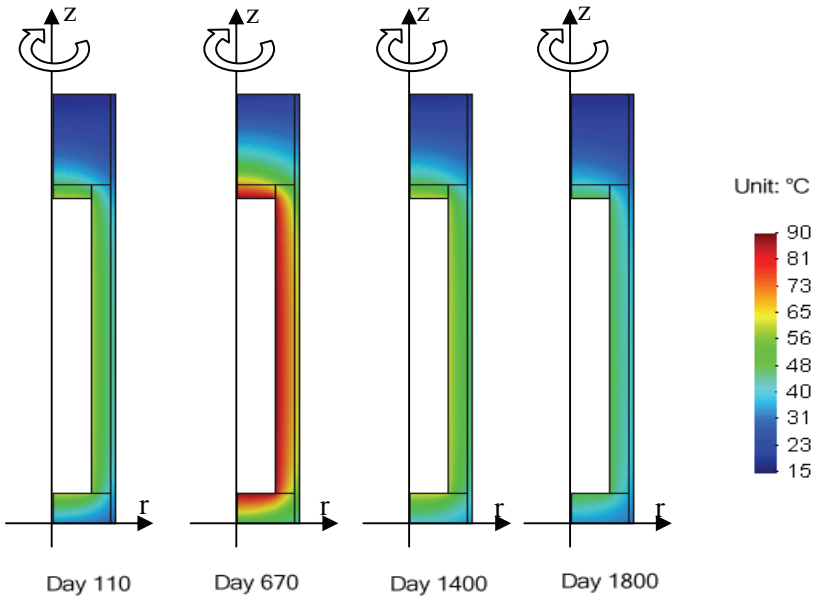

Figure 32: Simulated Temperature Contours in the Bentonite Ring, Bentonite Bricks, Bentonite Pellets and Cylindrical Bentonite at Four Different Times

4.2.1.2 Comparison of Temperatures between Simulated Results and Measurements in the Bentonite Materials

Figure 33 shows the comparison of the simulated temperatures with measurement at three different locations of T111, T121 and T112 on level R5. The simulated temperatures matched the measurements reasonably well at three different locations. After 900 days, the simulated temperatures were consistently lower than the measurements about 2~4°C. The reason is that there was no consideration of the influence of the nearby Temperature Buffer Test (TBT) when running in the numerical modelling. The TBT is another borehole-buffer-heater test that operated at very high temperatures. While the simulations did not take the TBT into account, the measurements made in the field were clearly influenced by the operation of that test.

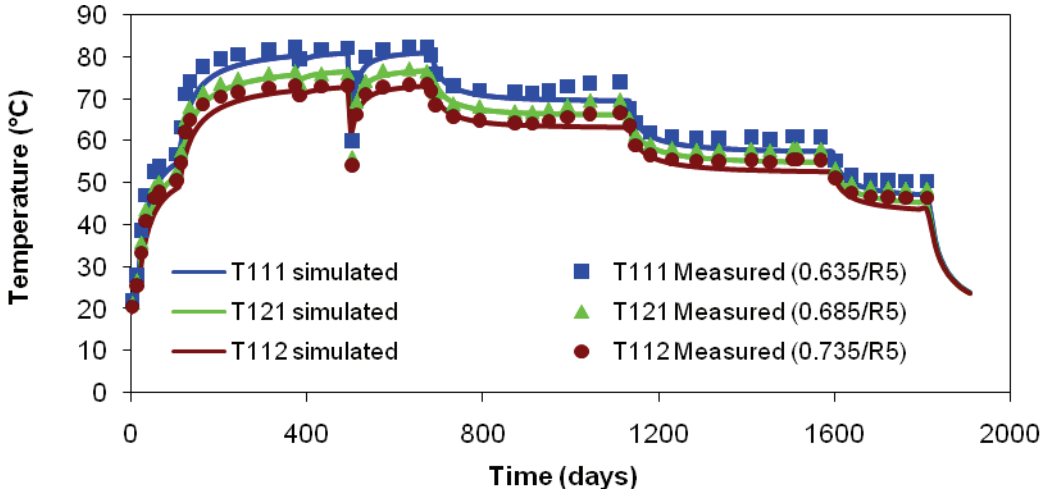

Figure 33: Comparison of Temperatures between Simulated Results from 2-D Model and Measurements at Sensors of T111, T121 and T112

Figure 34 shows the comparison of measured temperatures during the first 600 days and predicted temperatures after 600 days at three locations of W119, W120 and W121 on level R5. W119, W120 and W121 are 0.585 m, 0.685 m and 0.785 m from the axis of the container in R5 (refer to Figure 6 for locations). The simulated results matched the measurement very well during the first 600 days (after 600 days, the sensors broke down due to sudden decrease of temperature.

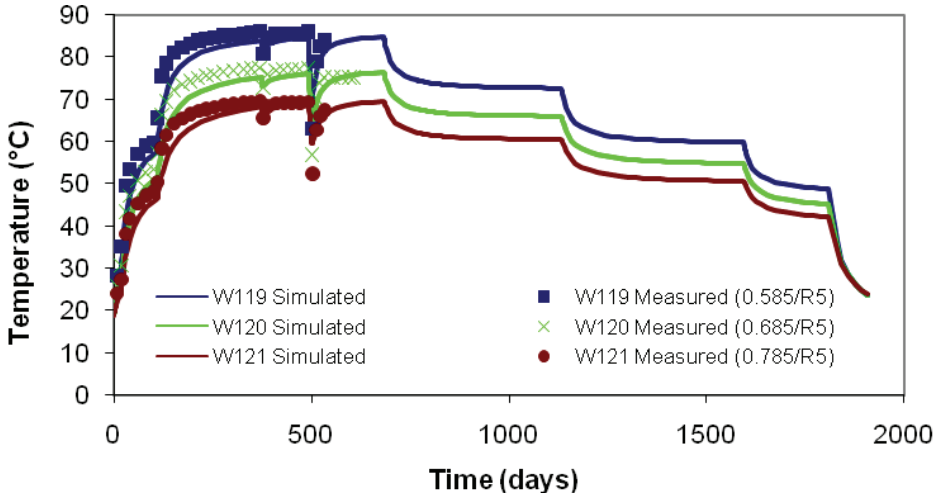

Figure 34: Comparison of Measured Temperatures and Predicted Temperatures during the First 600 Days at Sensors of W119, W120 and W121

Figure 35 shows the comparison of the simulated temperatures and measurements at locations of T127 and T129. T127 and T129 are 0.685 m from the axis of the container in R10 and 0.785 m from the axis of the container in C3 (refer to Figure 6 for locations). The simulated temperatures at location of T127 in level R10 were about 8°C higher than measurements. The reason probably was that the hydraulic parameter used for the bentonite bricks needs to be improved. The simulated temperatures at location of T129 matched the measurement reasonably well. After 900 days, the reason why the measurements at location of T129 were higher than the simulated results was that the simulated results did not incorporate the influences of the TBT running nearby.

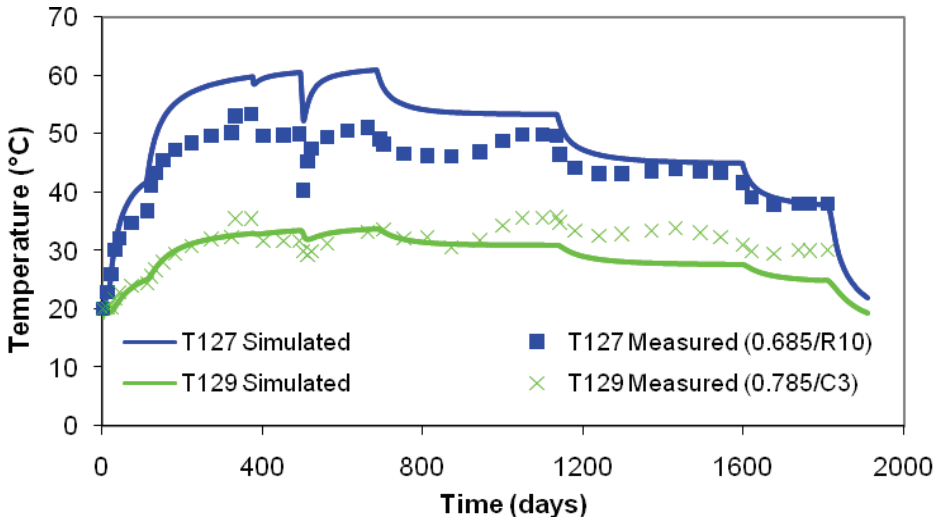

Figure 35: Comparison of the Simulated and Measured Temperatures at Two Different Locations T127 (in R10) and T129 (in C3)

4.2.1.3 Comparison of Temperatures between the Simulated Results and Measurements in the Rock

Figure 36 shows six different locations (TR105, TR108, TR117, TR120, TR129 and TR132) at which the temperatures in the rock were measured. Figures 37, 38 and 39 show the comparison of the simulated temperatures with measurements at different locations of TR105, TR108, TR117, TR120, TR129 and TR132. At different locations, the simulated temperatures matched measurements very well, indicating that the parameters used for the rock were reasonable.

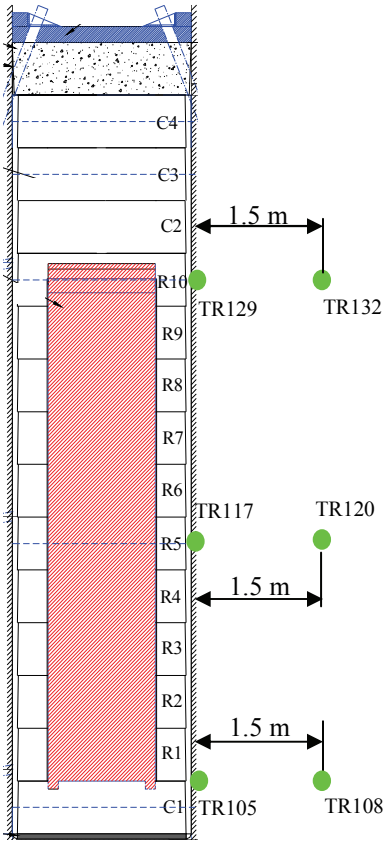

Figure 36: Locations at which Temperatures in the Rock were Measured

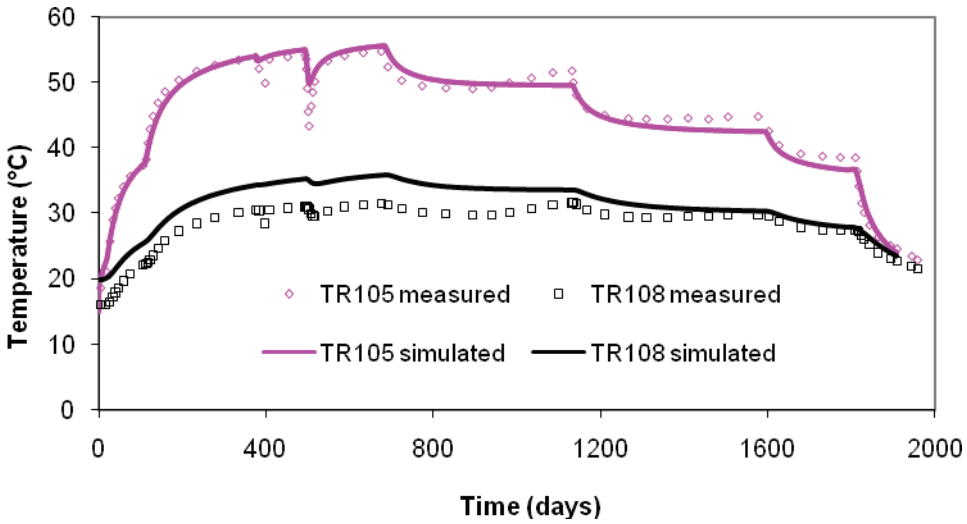

Figure 37: Comparison of Simulated Temperatures with Measurements at Locations of TR105 and TR108 in the Rock

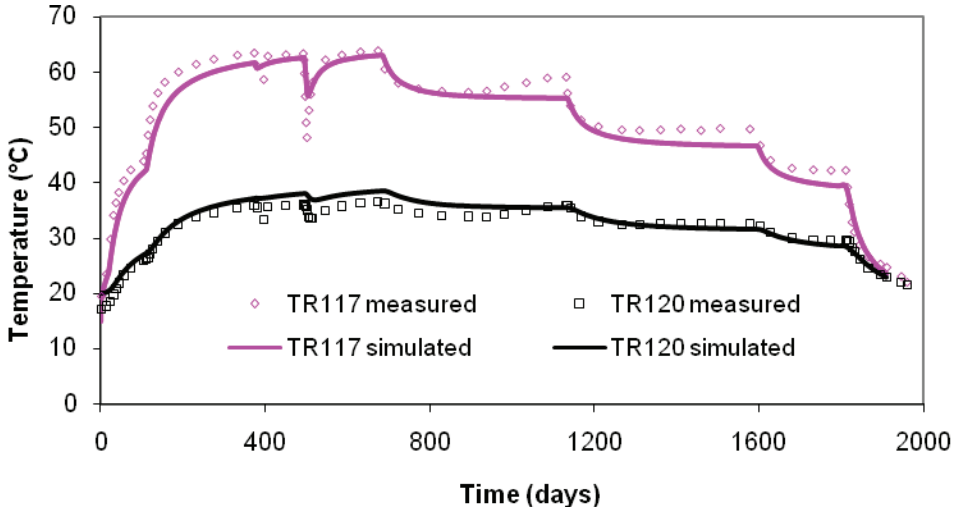

Figure 38: Comparison of Simulated Temperatures with Measurements at Locations of TR117 and TR120 in the Rock

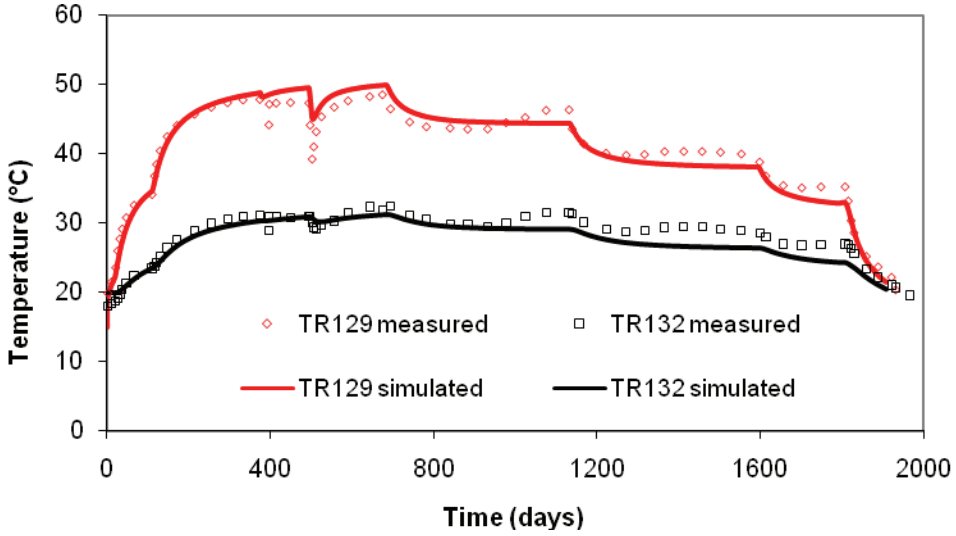

Figure 39: Comparison of Simulated Temperatures with Measurements at Locations of TR129 and TR132 in the Rock

4.2.2 Hydraulic Response

4.2.2.1 Simulated Hydraulic Response in the Bentonite Materials

Figure 40 shows water saturation histories at different locations on level R10 (see Figure 2 for locations), and Figure 41 shows the water saturation versus distance from the borehole axis at four different times. Earlier in the test the water saturation changed rapidly. After 1800 days, there was almost no change at the different locations. At the centre of the bentonite bricks (refer to Figure 3 for location) (0.05 m from the axis of borehole), the saturation increased from initial saturation of 0.637 to 0.783 on Day 1910.

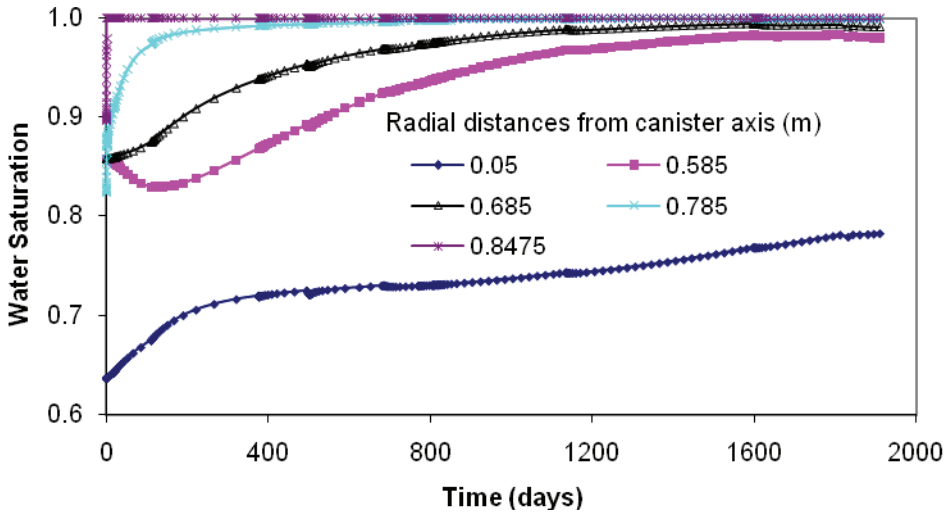

Figure 40: Simulated Water Saturation Histories at Different Locations along Level R10

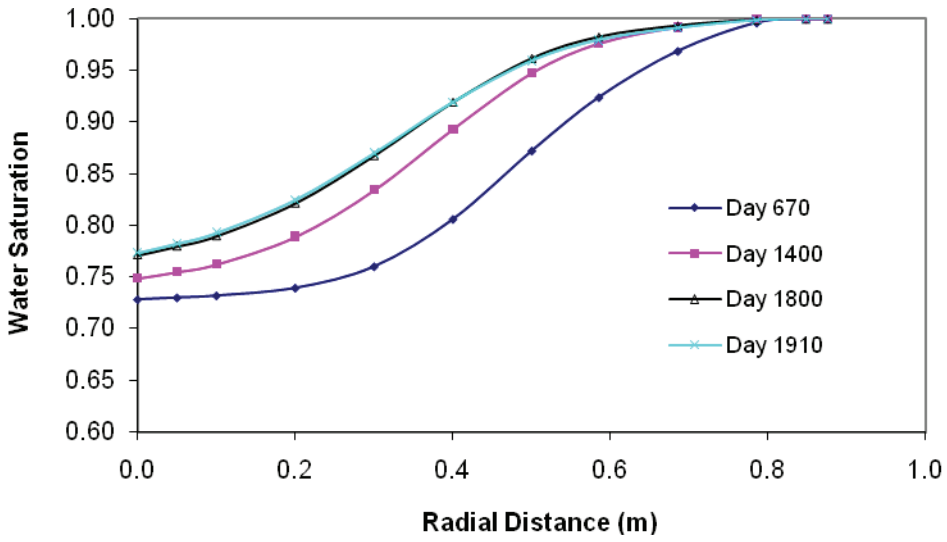

Figure 41: Simulated Water Saturation Profiles along Level R10

Figures 42 and 43 show water saturation histories at different locations and the water saturation profile at mid-height along a horizontal line in C3 (Refer to Figure 2 for locations) at four different times. At the centre of level C3, the water saturation increased from 0.756 to 0.8 on Day 1910.

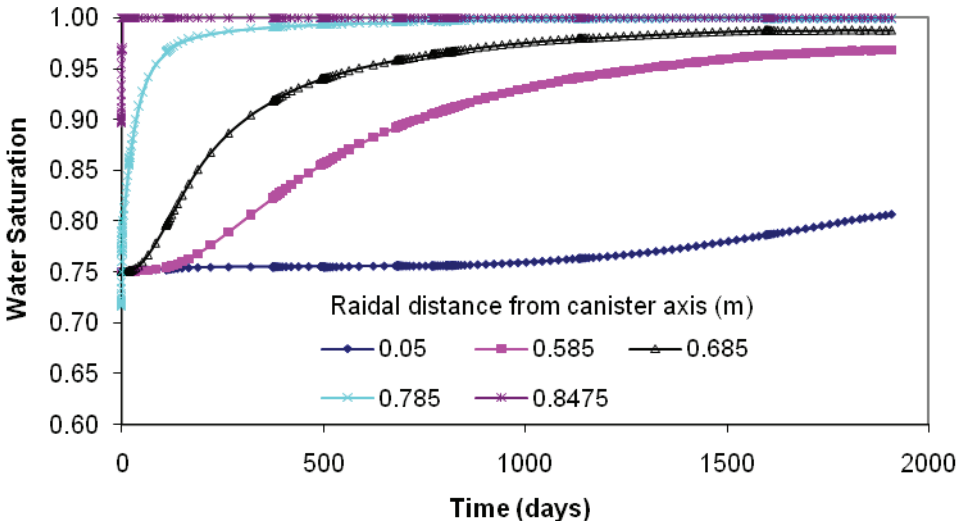

Figure 42: Simulated Water Saturation Histories at Different Locations along Level C3

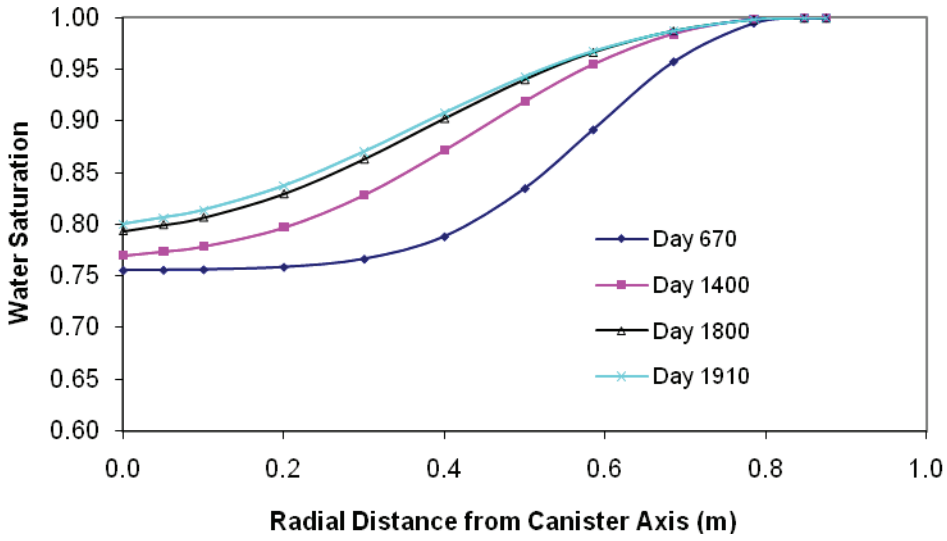

Figure 43: Simulated Water Saturation Profiles along Level C3

Figure 44 shows the pore water pressure in the ring-shaped bentonite blocks, bentonite bricks and cylindrical bentonite at four different times. On Day 1400, ring-shaped bentonite blocks were almost fully saturated. However, cylindrical bentonite blocks and bentonite bricks were far from saturated even after Day 1800.

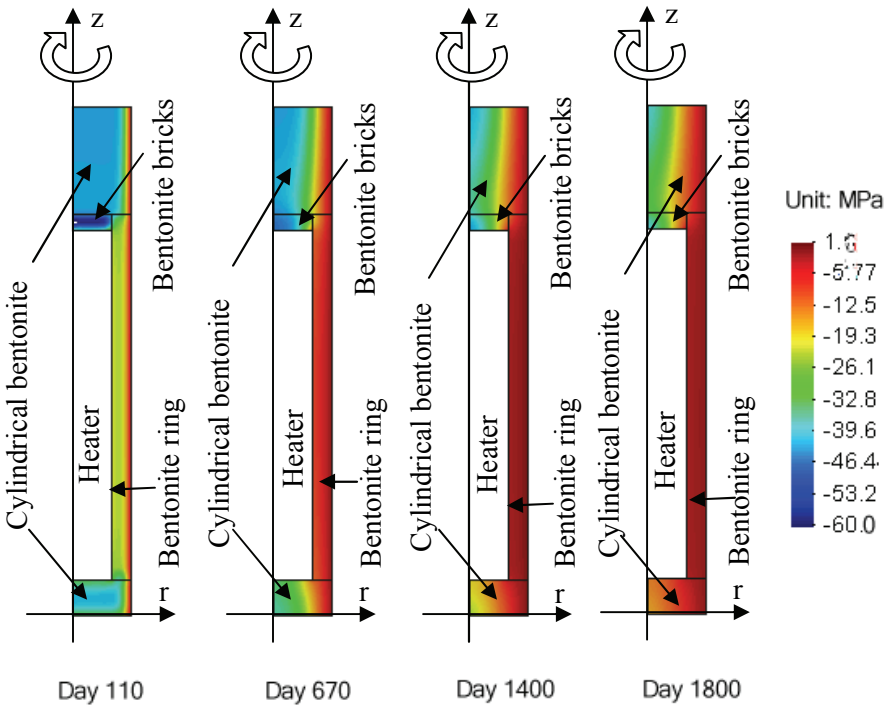

Figure 44: Simulated Pore Water Pressure Contours in the Bentonite Ring, Bentonite Bricks and Cylindrical Bentonite at Four Different Times

4.2.2.2 Comparison of Hydraulic Response between Simulated Results and Measurements

Figure 45 shows the comparison of simulated relative humidity at different locations with measurements in C3 (W151 and W153) and R10 (W134 (in bentonite bricks), W142 and W137). Except for W151, the simulated results matched the measurements reasonably well at different locations.

Figures 46 through 49 show the comparison of simulated water saturation profiles with measurements along levels R6, R7, R10 and C3 at the end of the test (Refer to Figure 2 for locations). For levels R6, R7 and R10, the simulated water saturation matched the measurements very well at different locations. For level C3, the simulated water saturation, general speaking, matched the measurements reasonably well.

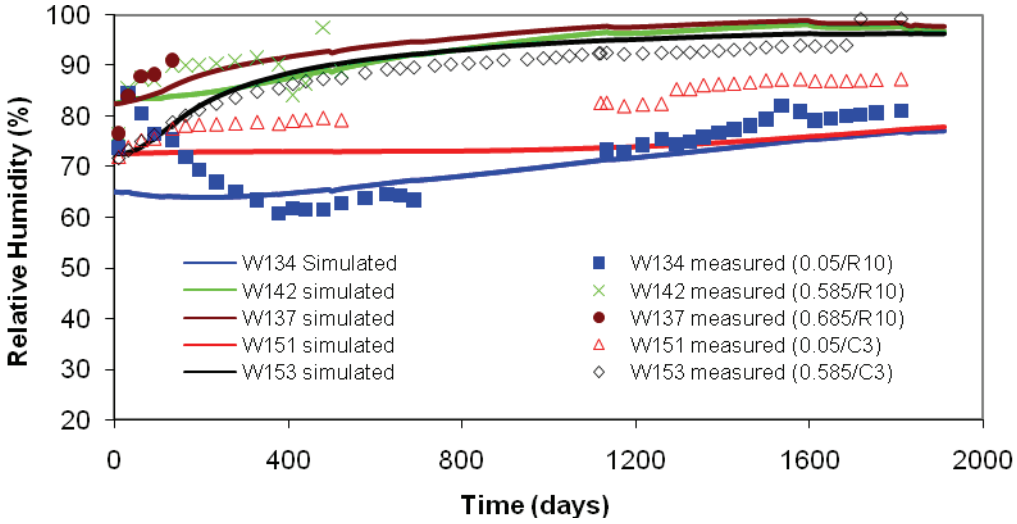

Figure 45: Comparisons of Simulated Relative Humidity with Measurements at Locations W134, W142, W137, W151 and W153

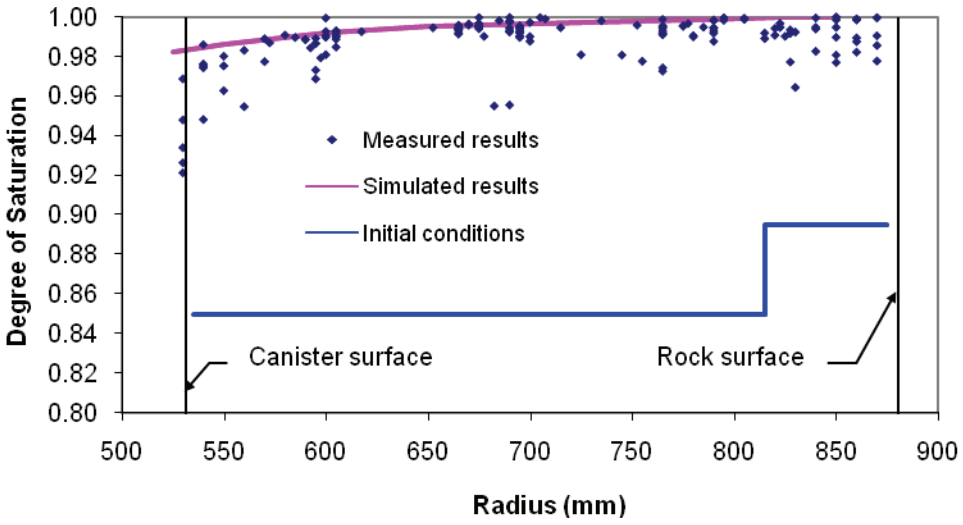

Figure 46: Comparison of Simulated Water Saturation with Measured Results along Level R6

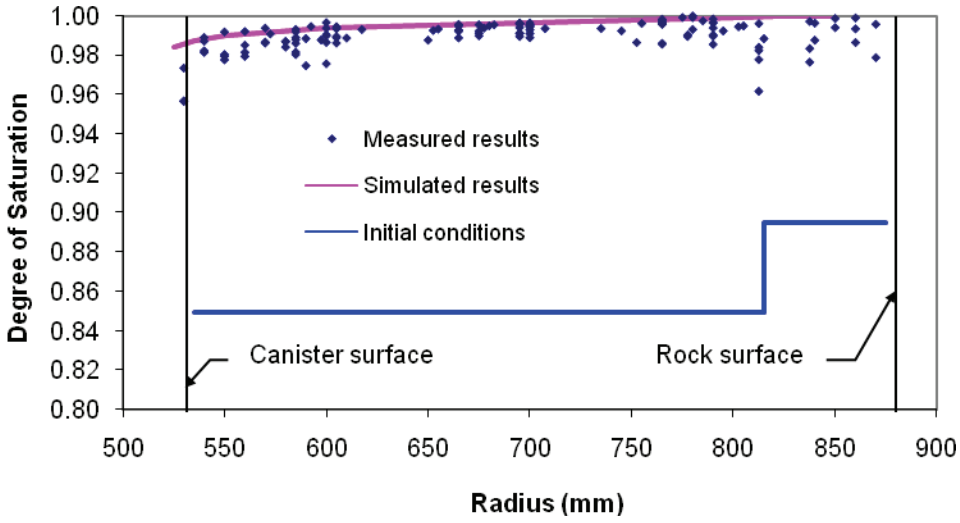

Figure 47: Comparison of Simulated Water Saturation with Measured Results along Level R7

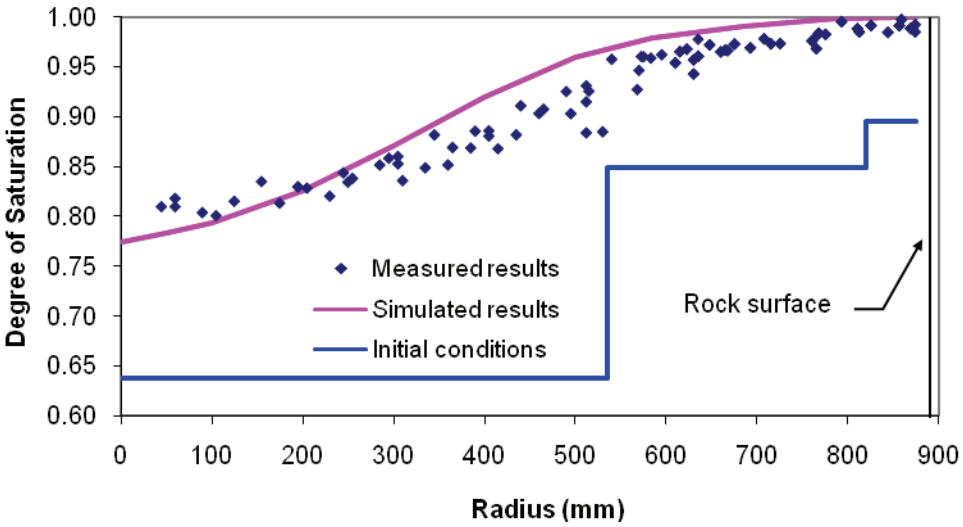

Figure 48: Comparison of Simulated Water Saturation with Measured Results along Level R10

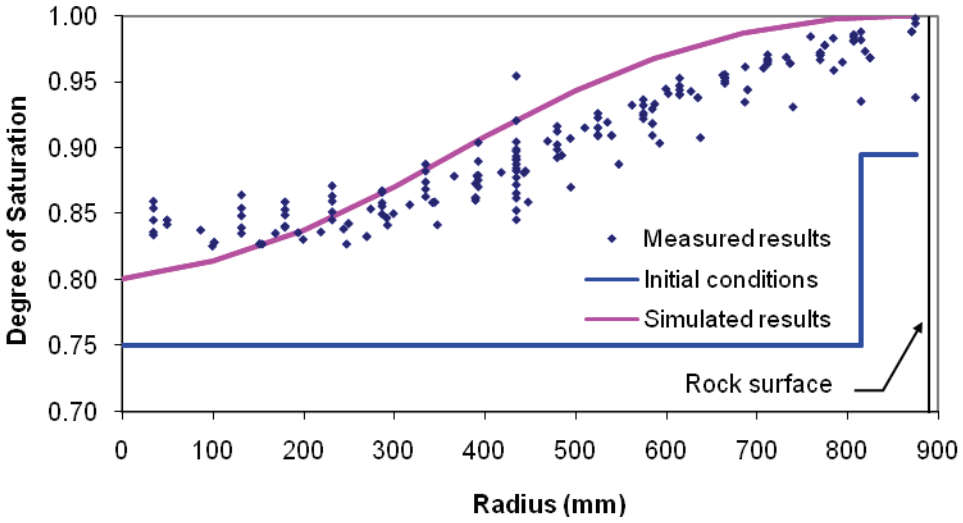

Figure 49: Comparison of Simulated Water Saturation with Measured Results along Level C3

Figure 50 shows the comparison of the simulated relative humidity with measurements during the first 600 days and predicted relative humidites after 600 days at location of W119, W120 and W121 (after 600 days, the sensors W119, W120 and W121 broke down). Like the results from one-dimensional modelling, the simulated relative humidity for W121 matched the measurement very well. The simulated relative humidity for W119 and W120 were lower than the measured results.

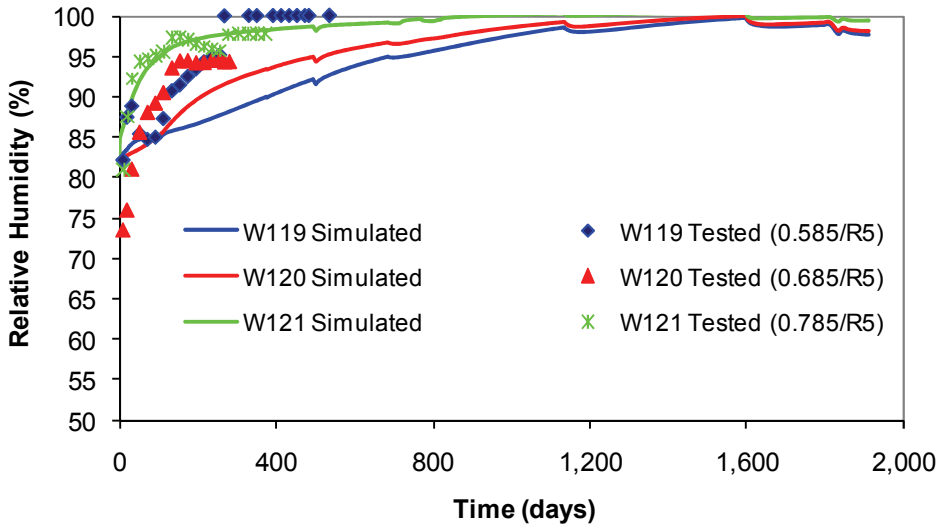

Figure 50: Comparison of the Simulated Relative Humidity with Measurements during the First 600 Days and Predicted Relative Humidity after 600 Days at Location of W119, W120 and W121

Figure 51 compares the simulated suctions with measurements at locations W122, W123 and W124 (Refer to Figure 6 for locations). Location W124 matched the pattern of the measurements reasonably well. However, locations W122 and W123 show significant differences in suctions values compared to the measured results.

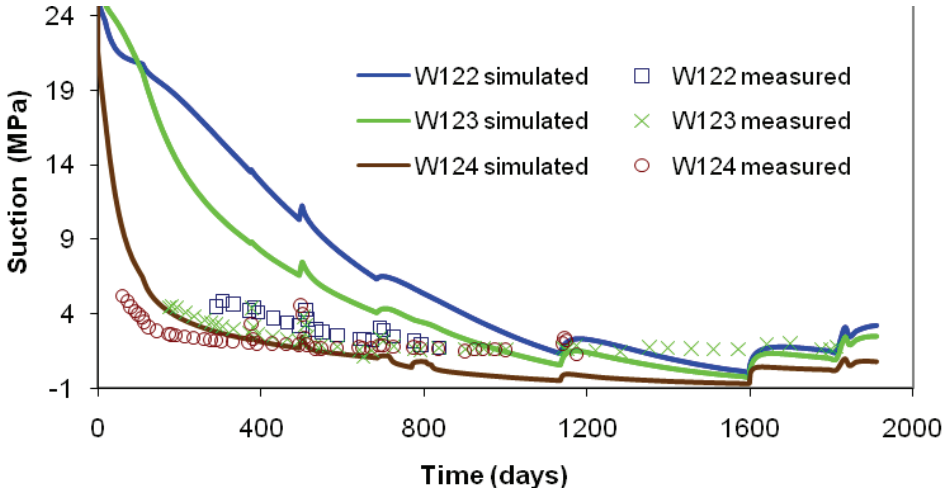

Figure 51: Comparison of the Simulated Suction with Measurements at Location of W122, W123 and W124

4.2.3 Mechanical Response

During coupled THM modelling, a convergence problem was encountered when the simulation reached 684 days after the start of the experiment. This was caused by the application of the boundary hydraulic pressure increase conditions, which might cause a greater tensile stress in the bentonite materials.

Figure 52 shows the comparison of the simulated vertical stresses with measurements at locations of sensors P110, P111 and U106. All of the simulated results were much lower than those measured. As discussed in one-dimensional modelled results, the differences in value indicate that there may be some as-yet unidentified feature or process that the model is not capturing accurately.

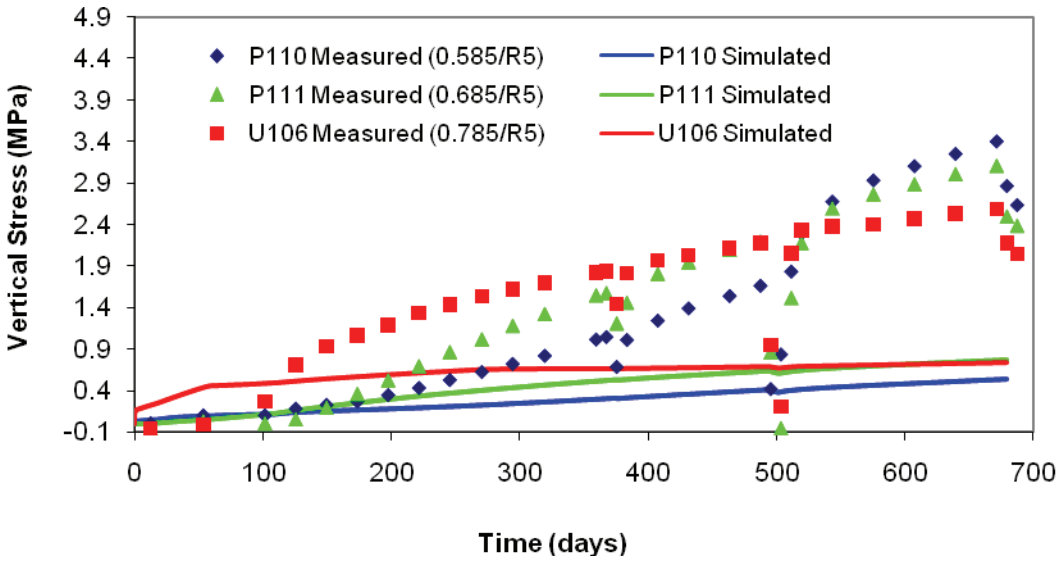

Figure 52: Comparison of the Simulated Vertical Stresses and Measured Results at Locations of P110, P111 and U106

Figure 53 shows the comparison of the simulated vertical stresses and measured results at locations of P119 in R10 and P125 in C3. Sensor P119 was located 0.685 m from the axis of the borehole along R10 and P125 was located 0.05 m from the axis of the borehole along C3 (refer to Figure 6 for locations). The simulated results matched the measurements reasonably well for both locations.

4.2.4 Summary of the Results from Two-Dimensional Modelling

In blocks R5 and C3, the simulated temperature matched the measurements well. In blocks R10, the simulated temperature was 8°C higher than the measurements during the early 900 days. Later on, the simulated matched the measured very well. In rock, the simulated temperatures matched the measurement very well at different locations.

In blocks R5, the simulated relative humidity matched the measurements reasonably well. The simulated suction matched measurements well for Sensor W124, not very well for Sensors W122 and W123. In blocks R10 and C3, the simulated relative humidity matched the measurement very well except for Sensor W153. In block R10 and C3, there were some obvious differences between the simulated suction and the measurement in value for Sensors W140 and W154.

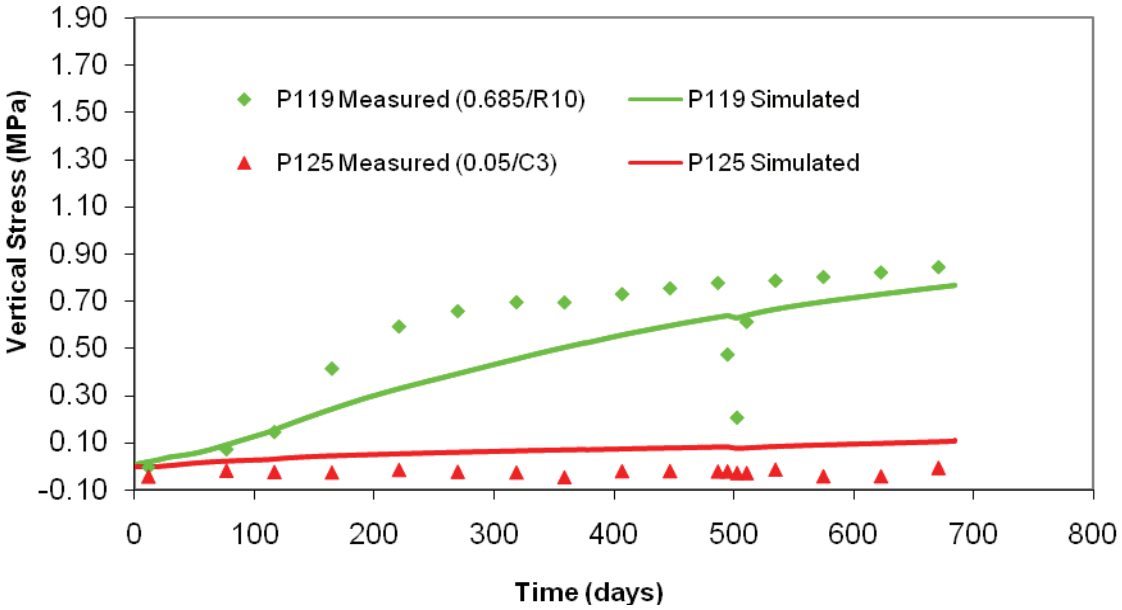

Figure 53: **Comparison of the Simulated Vertical Stresses and Measured Results at Locations of P119 and P125**

The simulated liquid saturation profiles matched the measurements very well at different layers (R6, R7, R10 and C3) at the end of tests.

The simulated vertical stresses at layer R5 caught the trends of measurements. However, the simulated results were smaller than measurements in value. The simulated vertical stresses at layer R10 and C3 matched measurements reasonably well.

4.3 COMPARISON OF MODELLING RESULTS FROM THE 1-D MODEL AND THE 2-D MODEL

Figure 54 shows the comparison of temperatures at three different locations from 1-D model and from 2-D model. During the first 800 days, the temperatures from the 1-D model were approximately 2~4°C higher than those from 2-D model. There are two reasons for this difference in temperature. One reason is that the adiabatic boundary conditions were applied on the top and the bottom of the 1D model. The second reason is that in 1-D model temperature boundary conditions were applied on the hot and cold ends, while heater power was applied on the nodes of heater in 2-D model. After approximately 800 days, the temperatures from 1-D model were about 6~7°C higher than those from 2-D model. Except for the reason causing the difference for the first 800 days, temperature boundary conditions based on measurements in 1-D model considered the influence of the TBT test, while in 2-D model the influence of the TBT test was not considered because the thermal load was applied using heater power.

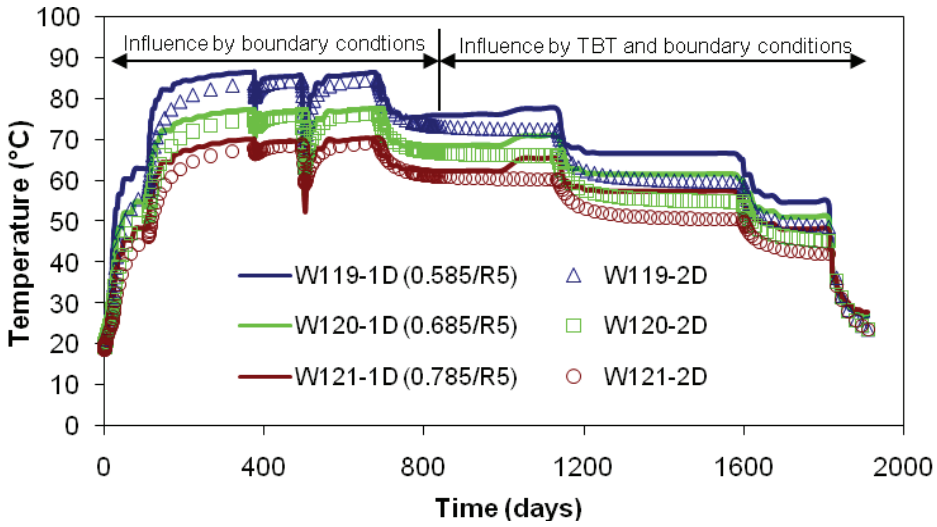

Figure 54: Comparison of Temperatures from 1-D Model and from 2-D Model

5. CONCLUSIONS

One-dimensional and two-dimensional coupled TH and coupled THM simulations for the CRT were conducted using CODE_BRIGHT. In this modelling activity, the following conclusions were determined.

1. Thermal responses were successfully modelled for the bentonite materials and the granite using either the coupled TH model or coupled THM model.

2. The hydraulic response could also be successfully modelled using coupled models.

3. The trends of mechanical response development could be captured in the simulations, however, there were some difficulties in obtaining a good match in absolute values.When a high pore water pressure boundary was applied to bentonite materials, there were some difficulties with convergence in coupled THM modelling because greater pore water pressure can cause greater tensile stress in the bentonite materials.

ACKNOWLEDGEMENTS

The author would like to thank Clay Technology AB of Sweden for supplying the data from the CRT experiment and the materials properties values for use in these numerical simulations. AECL technical reviews from D. Dixon, B. Holowick and D. Priyanto are appreciated.

REFERENCES

Alonso, E.E., A. Gens and A. Josa. 1990. A constitutive model for partially saturated soils. Geotechnique 40, pp. 405-430.

Borgesson, L. and J. Hernelind. 1999. Preliminary modelling of the water-saturation phase of the buffer and backfill materials. Äspö Hard Rock Laboratory. SKB IPR-00-11.

Borgesson, L., L.-E. Johannesson, T. Sandén and J. Hernelind. 1995. Modelling of the physical behaviour of water saturated clay barriers. Laboratory tests, material models and finite element application. SKB Technical Report 95-20.

Chandler, N.A. 2003. Numerical modeling of repository sealing systems as applied to the analysis of Underground Research Laboratory experiments. Ontario Power Generation Inc., Nuclear Waste Management Division Report 06819-REP-01200-10099-R00.

Dang, K.D. and J.-C. Robinet. 2004. Thermo-hydro-mechanical behaviour of MX80 bentonite for temperature $\geq 100°C$. Final Report, ANDRA Report C.RP.0EUG.02.008.

ENRESA. 2000. Full-scale engineered barriers experiment for a deep geological repository for high-level radioactive waste in crystalline host rock (FEBEX project). Nuclear Science and Technology Series, EUR 19147. Commission of the European Communities. Luxembourg, p. 362.

Gatabin C. and P. Billaud. 2005. Bentonite THM mock-up experiments sensors data report. CEA, NT DPC/SCCME 05-300-A.

Gens, A., A.J. Garcia-Molina, S. Olivella, E.E. Alonso and F. Huertas. 1998. Analysis of a full scale in situ test simulating repository conditions. Int. J. Numer. Anal. Mech. Geomech. 22, pp. 515-548.

Graham, J., N.A. Chandler, D.A. Dixon, P.J. Roach, T. To and A.W.L. Wan. 1997. The Buffer/Container Experiment: Results, synthesis, issues. Atomic Energy of Canada Limited, AECL-11746, COG-97-46-1.

Gray, M.N., S.C.H. Cheung and D.A. Dixon. 1985. Swelling pressures of compacted bentonite/sand mixtures. Material Research Society Proceedings. Vol. 44, pp. 523-530.

Hokmart, H. and B. Falth. 2003. Temperature buffer test. Predictive modelling programme. Äspö Hard Rock Laboratory Internal Report F12.1G 1012125.

Kristensson, O. and L. Börgesson. 2008 (In Prep). CRT – Canister Retrieval Test: Suggested EBS Task Force Assignments.

Thomas, H.R., P.J. Clean and T.A. Melhuish. 2003. Simulation of the Tunnel Sealing Experiment using HTM Modeling. Ontario Power Generation Inc., Nuclear Waste Management Division Report 06819-REP-01200-10112-R00.

Villar, M.V. 2002. Thermo-hydro-mechanical characterization of a bentonite from Cabo de Gata. A study applied to the use of bentonite as sealing material in high level radioactive waste repositories. Publicasión Técnica ENRESA 01/2002, p. 258, Madrid.

Villar M.V. 2003. AESOIE Hard rock laboratory. CIEMAT contribution to 2001 Annual Scientific Report. CIEMAT Internal Report CIEMAT/DIAE/54540/2/03.